LM CATHODE THRUSTER SYSTEM

QUARTERLY PROGRESS REPORT NO. 1, PHASE II

18 JULY 1969 through 4 OCTOBER 1969

CONTRACT JPL 952131

by

J. HYMAN, JR., J.R. BAYLESS,

D.E. SCHNELKER, J.W. WARD, and R.L. SELIGER

15 OCTOBER 1969

HUGHES

HUGHES AIRCRAFT COMPANY

RESEARCH LABORATORIES

MALIBU, CALIFORNIA
90265

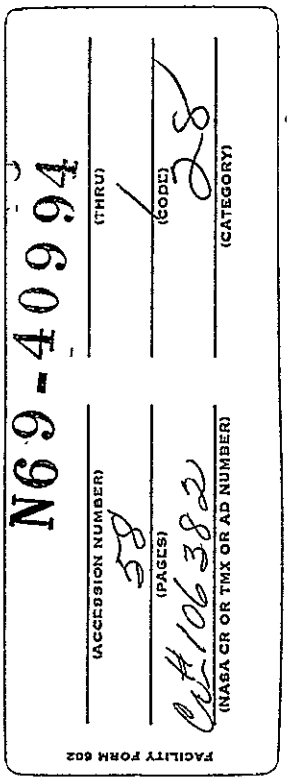

HUGHES RESEARCH LABORATORIES
Malibu, California

a division of hughes aircraft company

LM CATHODE THRUSTER SYSTEM

Quarterly Progress Report No. 1, Phase II
18 July 1969 through 4 October 1969
Contract No. JPL 952131

J. Hyman, Jr., J.R. Bayless,
D.E. Schnelker, J.W. Ward, and
R.L. Seliger

15 October 1969

Performed for

Jet Propulsion Laboratory
California Institute of Technology

Sponsored by

National Aeronautics and Space Administration
Contract NAS 7-100 (Task Order #RD-26)

This report contains information prepared by the Hughes Research Laboratories under JPL subcontract. Its content is not necessarily endorsed by the Jet Propulsion Laboratory, California Institute of Technology, or the National Aeronautics and Space Administration.

TABLE OF CONTENTS

LIST OF ILLUSTRATIONS

ABSTRACT

A 20 cm LM cathode thruster system is being developed for operation at beam currents I_B = 0.5 A to 1.0 A and a beam voltage V_B = 2 kV. Fabrication of the components of the thruster and ground-screen shroud is nearing completion. The thermal design and the thin-screen high-transparency ion-extraction system are similar to those in use with the 30 cm LM cathode thruster developed during the previous phase of this contract. The discharge chamber configuration is derived from that of a 20 cm thruster with an externally cooled LM cathode which is now being optimized for operation in the desired current range. Best performance to date has been achieved at I_B = 790 mA and V_B = 2 kV with a source energy per ion V_S = 290 eV/ion at a mass utilization efficiency η_m = 88%. A lightweight LM cathode has been fabricated, and a feed system is being developed which consists of an electromagnetic pump, a liquid-mercury flowmeter, and a high-voltage isolator. The pump generates a pressure rise of ±0.6 atm with a power expenditure of 2 W, and the flowmeter shows promise of a measurement accuracy of ±1%. All subsystems are enclosed within the ground-screen shroud. The entire system is thermally integrated and rejects discharge heat by radiation alone.

SECTION I

INTRODUCTION

For detailed mission analysis or comparative evaluation of alternative thruster types, it is necessary to know the operating characteristics of an entire thruster system, including the subsystems for propellant feed, ion beam neutralization, and power conditioning. The development of each of these components for the LM cathode thruster system has now reached a stage where a laboratory-type thruster system (not involving flight-type power supplies) can be built based on existing technology. As a first step in the construction of this system, a thermally integrated 20 cm LM cathode thruster is being designed for operation at beam currents I_B = 0.5 A to 1.0 A. A mercury feed system is also being designed and fabricated which consists of a single-capillary flow impedance, a differential pressure transducer (to determine mercury flowrate), an electromagnetic pump, and a hydrogen-bubble high-voltage isolator. The feed system is enclosed within the ground-screen shroud of the thruster and operated as part of a complete thruster system. The resulting unit requires only a mercury supply and the appropriate electrical power for its operation. No neutralizer cathode development is planned under this effort.

Programs for research and development of the LM cathode, the thruster, and various elements of the liquid-mercury feed system have been carried out as separately funded projects. Through coordinated guidance of the over-all program, however, these separate projects have produced the necessary devices and technology which will lead to the development of a reliable and useful laboratory-type thruster system.

The feasibility of LM cathode thruster life in excess of 10^4 hours was demonstrated at Hughes Research Laboratories (HRL) under Contract NAS 3-6262; a 20 cm thruster equipped with a circular LM cathode was successfully tested for an accumulated 4,000 hours. No erosion of the molybdenum cathode structure was evident following this test and no degradation of the cathode performance occurred. Development of high-temperature LM cathodes began at HRL under Contract NASW-1404 after it became apparent from thermal analysis that combining thrusters in peripheral or clustered arrays places a constraint on the operation of any electron-bombardment ion thruster unless the temperature of the thruster shell can be permitted to exceed a value on the order of 200°C.

The demonstrated feasibility of system life in excess of 10^4 hours, combined with a demonstrated capability for operation of a high-temperature LM cathode in an efficient thruster, prepared the way for the construction of a 30 cm thermally integrated thruster under the current contract. This thruster has now demonstrated efficient performance at a specific impulse $I_{sp,eff}$ = 4,100 sec; a beam current I_B = 1,400 mA is produced at a beam voltage V_B = 2 kV with a source energy per ion V_S = 270 eV/ion* at a mass utilization efficiency η_m = 90%. At this power level, the thermally integrated LM cathode achieves an equilibrium body temperature T_K = 200°C; it rejects the heat from the discharge along a tapered aluminum endplate to the outer thruster shell, from which the heat is radiated to the walls of the vacuum chamber.

In a related contract effort (Contract NAS 7-539), the design of liquid-mercury feed systems was explored in detail. A number of unique components were built so that their operating characteristics could be established and the various systems which were considered could be properly evaluated. Two of these components, an electromagnetic (EM) pump and a high-voltage isolator, have since been incorporated into a breadboard flow system which was operated under the current contract for a final demonstration of the proper operation of each of the components and of the mutual compatibility of all of the components of the system. The feed system consisted of (1) a gas-pressurized positive-expulsion mercury reservoir, (2) the EM pump, (3) the liquid-mercury high-voltage isolator, (4) a single-capillary flow impedance, and (5) a high-temperature LM cathode which was thermally integrated with the 30 cm electron-bombardment thruster. Successful operation of the 30 cm LM cathode thruster with the breadboard liquid-mercury feed system led to the present development of a 20 cm LM cathode thruster system.

*V_S, the total source energy per ion, is the discharge energy per ion, because no heater, vaporizer, or keeper power is required with the LM cathode.

SECTION II

DESIGN OF THE 20 CM THRUSTER SYSTEM

Design of the 20 cm LM cathode thruster system is complete, and the components are now being fabricated. The thruster is designed to operate at beam currents I_B = 0.5 A to 1.0 A, and to dissipate by radiation all heat resulting from discharge losses. The discharge chamber configuration was modified only slightly (see Section IV-A) from that of the 20 cm thruster developed during the earlier phase of this contract, which is operated with an externally cooled LM cathode. The thermal design and the thin-screen, high-transparency ion extraction system are similar to those in use with the 30 cm thruster developed at the same time.

An isometric drawing of the 20 cm thruster system is shown in Fig. 1. Although the thruster and its liquid-mercury feed system are characteristically enclosed within a single ground-screen shroud, provision has been made in this design to allow the two subsystems to operate as separate units. (This permits the separate development of the feed system to proceed simultaneously with the optimization of the thruster prior to integration of the thruster system.) A screened enclosure extends the accel electrode and completes the enclosure formed by the ground screen. Although no neutralizer development is planned under this contract, provision has been made for mounting an LM cathode neutralizer over a sheet-metal extension of the ground screen which covers one quadrant of the accel-extension screen. The discharge igniter electrode and elements of the liquid mercury feed system are indicated in the drawing. Table I lists and gives the estimated weights of the components of the 20 cm thruster system. The total weight (including the thruster and ion-extraction system, the liquid-mercury feed system, and the ground-screen shroud) is approximately 5 kg.

A. THRUSTER DESIGN

The basic configuration of the discharge chamber of the thermally integrated thruster is similar to that of the 20 cm thruster developed under the earlier phase of this contract,[1] which uses an externally cooled LM cathode. Optimization of this thruster has continued under the current phase of the contract and is described in Section IV-A. The discharge chamber design for the thermally integrated thruster, shown in Fig. 2, is identical to that which thus far has been found to yield optimum performance in operation of the thruster which has an externally cooled

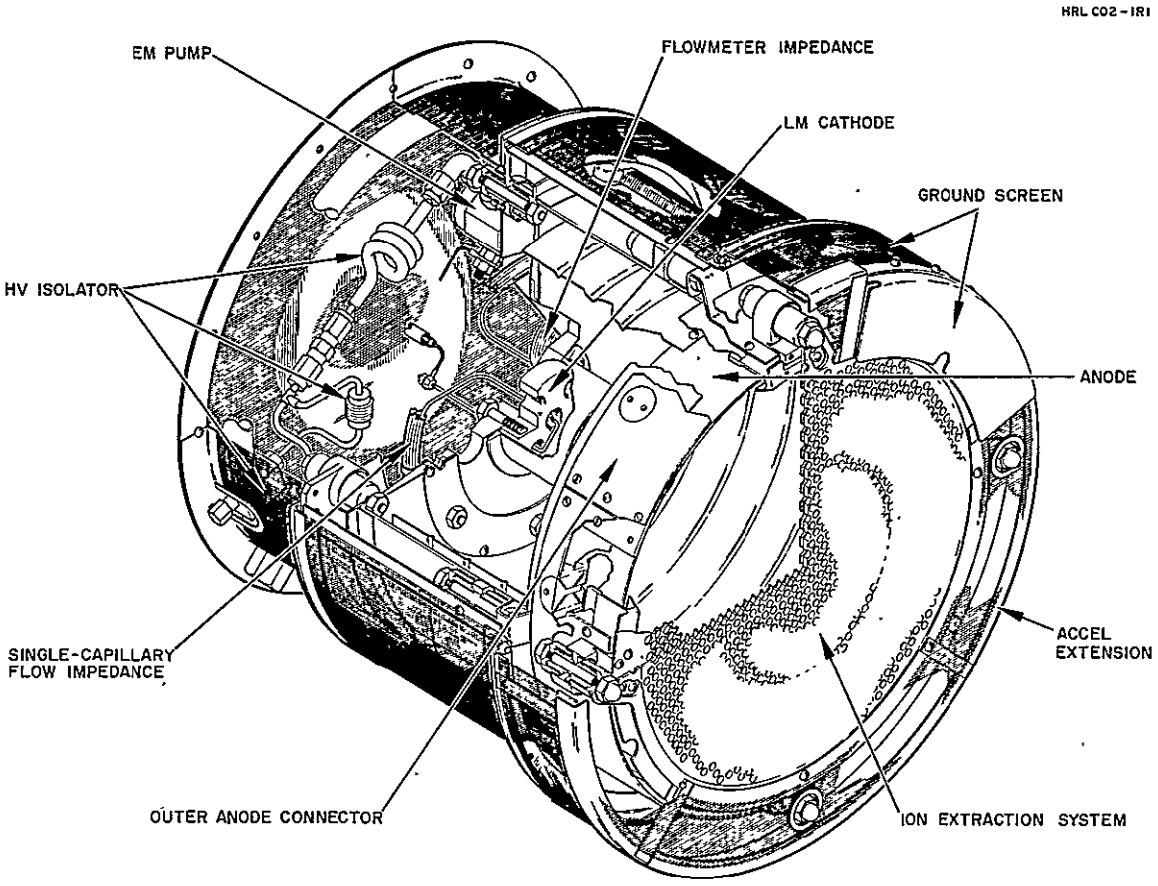

Fig. 1. Isometrid drawing of the 20 cm LM cathode thruster system.

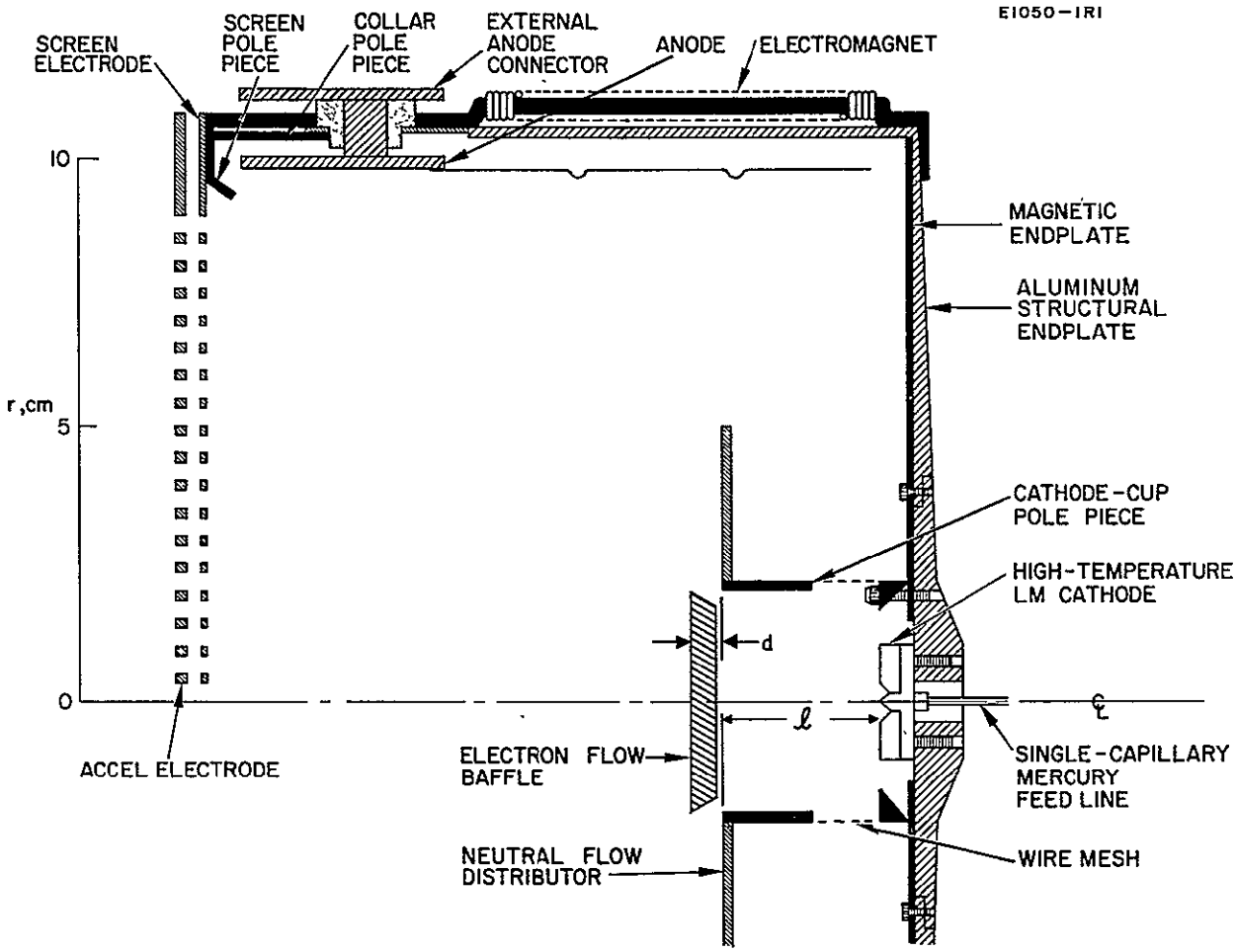

Fig. 2. Schematic cross section of the thermally integrated 20 cm LM cathode thruster.

TABLE I

Component Weights of the 20 cm Thruster System (Estimated)

Component	Part No.	Quantity per Assembly	Weight of Part, kg	Weight of Assembly, kg
Thruster				
Thruster Shell Assembly	839924	1	0.476	0.476
Band, Anode Feedthrough	839925	1	0.054	0.054
Anode, Upstream	839926	1	0.099	0.099
Anode, Downstream	839927	1	0 072	0.072
Outer Anode Connector	839928	1	0 086	0.086
Ceramic Spacer	839929	8	0.001	0.010
Accel. Electrode	839930	1	0 353	0.353
Stud	839931	4	0 006	0 024
Shield Insulator	839932	8	0 002	0.016
Bracket, Insulator, Center	839933	4	0.007	0 031
Support, Insulator, Accel.	839934	4	0.015	0.060
Support, Magnet, Upstream	839937	1	0.132	0.132
Splice Plate Assembly	839938	1	0 004	0.004
Pole Piece, Outer, Upstream	839940	2	0.068	0 136
Pole Piece, Inner, Upstream	839941	2	0.023	0 046
Pole Piece, Upstream Cover	839942	1	0.057	0.057
Screen Electrode	839946	1	0 127	0.127
Screen Pole Piece	839947	1	0.308	0 308
Magnet	839948	8	0.068	0.544
Nut & Screw-Mtg. Anode Sink	1024015	16	0.003	0.048
Ceramic Insulator, Feedthrough	1024016	8	0.013	0.104
Feedthrough, Anode	1024017	8	0.005	0.040
Screw, Shouldered	1024018	8	---	0.002
LM Cathode K-54	---	1	0.131	0.131
Total				2.960
Feed System				
Plate, Feed System Support	1024127	1	0.036	0.036
Mount, Transducer	1024129	1	0.002	0.002
Mount - LM Pump	1024130	1	0.003	0 003
Gasket - Isolator Connector	1029131	1	0 001	0.001
Retaining Nut Isolator Connector	1029132	2	0.004	0.008
Retaining Screw Isolator Connector	1029133	2	0 002	0 004
Connector Isolator	1029134	2	0.005	0 001
Hydrogen Reservoir	1024145	1	0 226	0 226
Isolator		1	0.028	0.028
EM Pump		1	0.301	0 301
Pressure Transducer		1	0.098	0 098
Hydrogen Diffuser		1	0.016	0 016
"Swagelok" Couplings		6	0.050	0.300
Plate, Feed System	1024059	1	0.098	0.098
Capillary Impedance	---	10m		0.083
Total				1.205
Ground-Screen Shroud				
Accel. Extension	1024019	1	0 094	0.094
Ground Screen, Center	1024020	1	0.240	0 240
Ground Screen, Optics Insulator	1024021	1	0.130	0 130
Ground Screen Neutralizer Cover	1024022	1	0.017	0.017
Ground Screen, End Cover	1024024	1	0.065	0.065
Ground Screen, Feed System	1024114	1	0 157	0.157
Stud	839931	8	0.006	0.048
Shield Insulator	839932	16	0.002	0.032
Ceramic Spacer	839929	16	0 001	0.020
Support, Insulator, Center	839935	4	0 003	0.012
Support, Insulator, Upstream	839936	4	0 006	0.024
Total				0.839
Total Weight of Assembly				5 004 kg

LM cathode. The anode diameter of the new thruster is 20 cm and the length of the discharge chamber from screen to end plate is 16.5 cm. The anode is segmented into two parts: a thermally conductive aluminum portion in the region closest to the screen electrode and a thin, nonconductive, stainless-steel portion extending over the upstream two-thirds of the anode. The thermally conductive portion of the anode is attached to an external connector by a series of leadthroughs consisting of short aluminum rods which pass through insulating ceramic sleeves. These leadthroughs serve the dual purpose of connecting the anode to the external electrical circuits, and conducting to the external connector the discharge heat which is delivered to the anode. The anode heat (which constitutes the major fraction of the total source power) is dissipated by radiation to space from the outer surface of the external anode connector and through the apertures of the ion-extraction system.

Discharge heat, which is generated at the cathode, passes from the molybdenum body of the LM cathode directly into the aluminum endplate of the thruster. This endplate is tapered to present a uniform thermal resistance per unit radial length for heat flow from the cathode to the cylindrical aluminum wall of the thruster, which continues the thermal path forward to the upstream edge of the external anode connector. Downstream of this position, the thruster body is constructed of a thin band of stainless steel which reduces conductive coupling between the cathode and anode thermal circuits. A lightweight iron endplate lies over the inner surface of the aluminum structural endplate to complete the magnetic circuit from the cathode pole piece to the electromagnets. Instead of a single iron sheet of the minimum thickness required to link the magnetic flux, the magnetic endplate consists of two thinner iron sheets. These sheets act as heat shields to further reduce the radiant coupling between the anode and cathode thermal circuits. As requirements dictate, the coupling can be reduced still further by placing additional heat shields between the anode and the inside surfaces of the aluminum thruster body.

The thickness of the aluminum structure was chosen as a compromise between the opposing requirements for good thermal conduction between cathode and lateral thruster wall and for light weight. As in the 30 cm thruster, the cylindrical wall is fabricated to a thickness of 0.150 cm. The aluminum endplate is 0.150 cm thick where it joins with the cylindrical aluminum wall, and increases in thickness inversely with the radius up to the point of attachment of the LM cathode.

Aluminum was chosen as the major structural material because of its combined properties of light weight and high thermal conductivity, which together have resulted in the design of a lightweight thermally integrated thruster. Initially the decision was made to employ aluminum for fabrication of the 30 cm thruster, with the understanding that under certain conditions in air mercury is known to attack aluminum in a highly

destructive manner. The literature[2] indicates, however, that alloys of aluminum with low silicon content have shown good resistance to such attack. Experience at HRL[3-5] led to the choice of low silicon content 6061 aluminum alloy as the major structural material for thruster fabrication. To date, no mercury attack has been observed in the 30 cm thruster after 200 hours of operation and 4,000 total hours of exposure to mercury.

Design of the 20 cm ion-extraction system is based primarily on the same criteria which determined the design of the existing 30 cm system,[1] which has performed satisfactorily throughout its 200 hours of accumulated operation. The hole pattern has been modified only slightly from that of the 30 cm system and is now identical with that used by Masek and Pawlik at JPL.[6] The plate thicknesses and the hole pattern and shape of the ion-extraction apertures are described in Table II.

TABLE II

Design Specifications for the Ion-Extraction System

Electrode	Material	Thickness, cm	Hole Diameter, cm	Distance Between Hole Centers, cm	Hole Shape
Screen	Molybdenum	0.076	0.475	0.535	Circular
Accel	Molybdenum	0.254	0.365	0.535	Circular

Two sets of ion-extraction electrodes have been fabricated. The accel electrode of one set has a uniform thickness, while that of the second set is tapered to a thickness of 0.127 cm at the outer diameter. The accel electrode is supported by four insulating supports on a bolt circle of 24.4 cm, which is compatible with that used at JPL.

The thruster magnetic field is generated by eight electromagnets spaced uniformly around the exterior of the discharge chamber. This number of electromagnets was chosen as being few enough to provide sufficient space for mounting of other thruster components and yet numerous enough to generate an azimuthally uniform magnetic field within the discharge chamber. The screen pole piece for the new 20 cm thruster is scaled from the design of the NASA SERT-II thruster.[7] An alternative screen pole piece has also been constructed with a configuration similar to that employed at JPL.[6]

A new single-capillary fed, high-temperature, annular LM cathode designated K-54 has been constructed for use with the 20 cm thruster. As shown in Fig. 3, its construction is very similar to that of LM cathode K-51 used earlier with the 30 cm thruster, except that the throughbolts previously employed to attach the cathode to the thruster endplate are replaced by studs which protrude only from the back of the cathode. With this design, only molybdenum cathode surfaces are exposed to the discharge. Holes are provided through the cathode body to provide clearance for a discharge igniter electrode.

B. FEED SYSTEM DESIGN

To supply propellant to the 20 cm thru... prototype liquid-mercury feed system has been designed with emphasis on simple, reliable operation. As shown in Fig. 4, the system contains all elements necessary to provide mercury propellant for the 20 cm LM cathode thruster in a measured and controllable manner. In order of flow sequence, the liquid-mercury feed system includes a mercury shutoff valve, the hydrogen-bubble high-voltage isolator, the EM pump, a mercury flowmeter, and a single-capillary impedance to regulate the mercury flow to LM cathode K-54.

The feed system is supplied with mercury by a gas-pressurized mercury reservoir (shown in Fig. 5). Pressurized nitrogen is applied above a piston pressing on the mercury surface to serve as the driving force. The piston position is indicated by a dial indicator (calibrated to 0.001 in. or 0.001 in.) which contacts the top of the piston shaft, and its displacement as a function of time serves as an indication of mercury consumption and yields an accurate measure of the flowrate which supplements the instantaneous value obtained from the flowmeter. The shutoff valve permits handling of the thruster system outside the vacuum environment with no loss of mercury or atmospheric contamination of the stored mercury. The high-voltage isolator permits operation of the thruster at a potential which is different from that of the propellant storage reservoir. Mercury pressure can be regulated, as needed to control the mercury flowrate, by means of an electromagnetic pump; the single-capillary flow impedance establishes a mercury flowrate which is linearly related to the applied pressure. The characteristics of the single-capillary flow impedance are sufficiently linear and repeatable to permit its use for both flow control and flow measurement.[1] A differential pressure sensor, which measures the pressure drop across a calibrated segment of the single-capillary flow impedance, provides instantaneous electrical readout of the mercury flowrate. This electrical readout, combined with the capability for electrically actuated pressure regulation, will allow the flow system to be incorporated with external automatic flow controllers in the future.

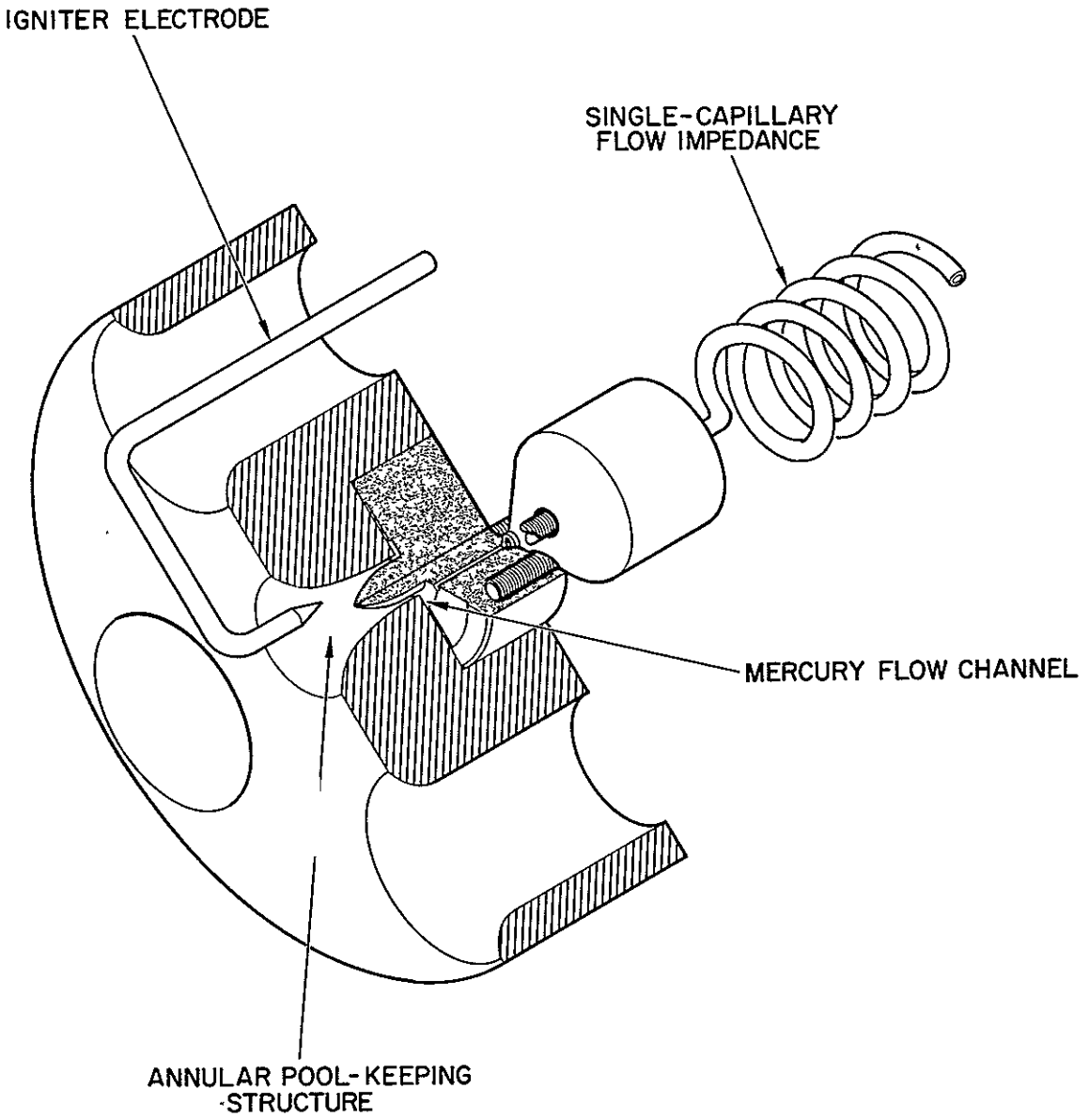

Fig. 3. LM cathode K-54.

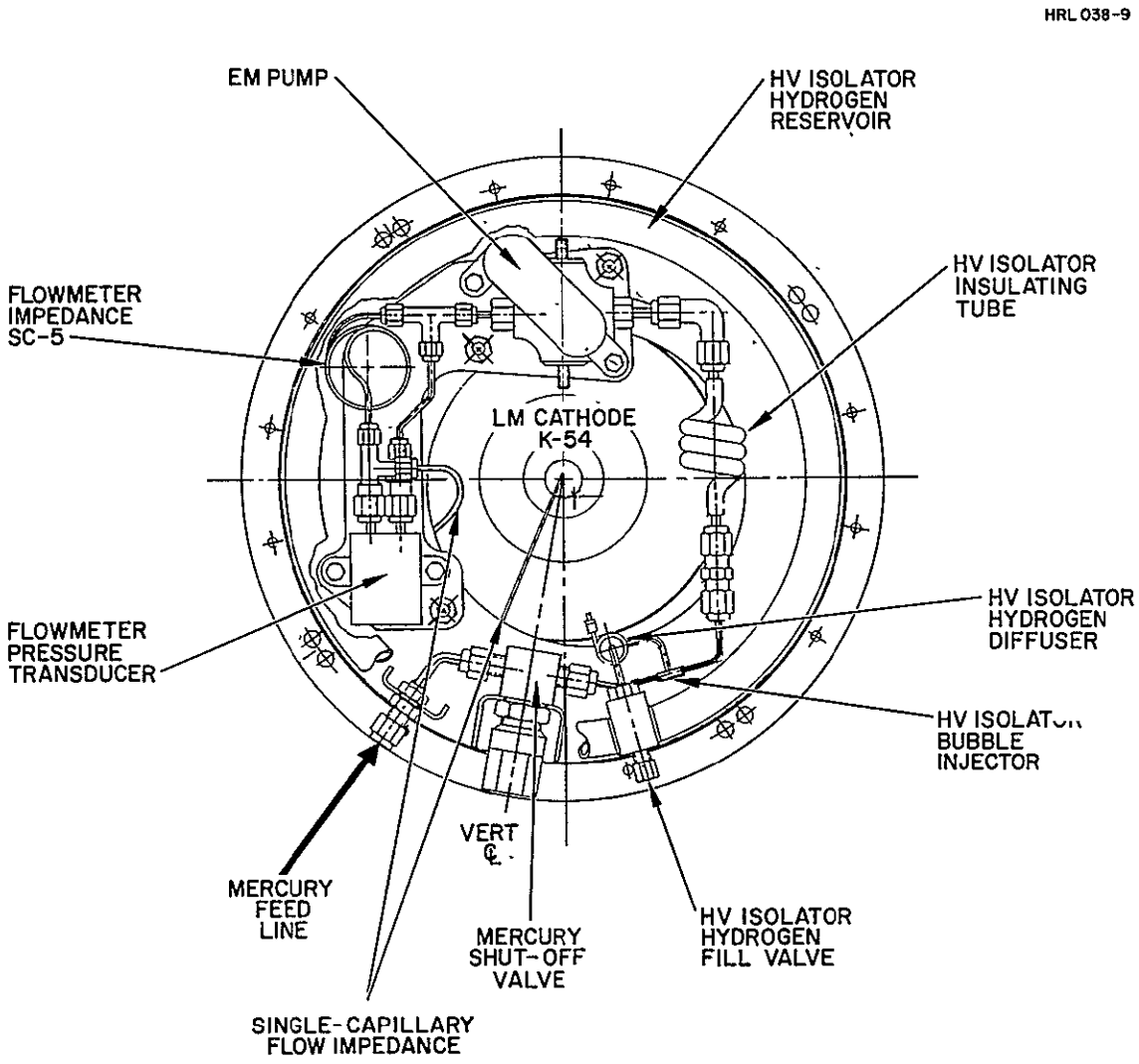

Fig. 4. Liquid mercury feed system.

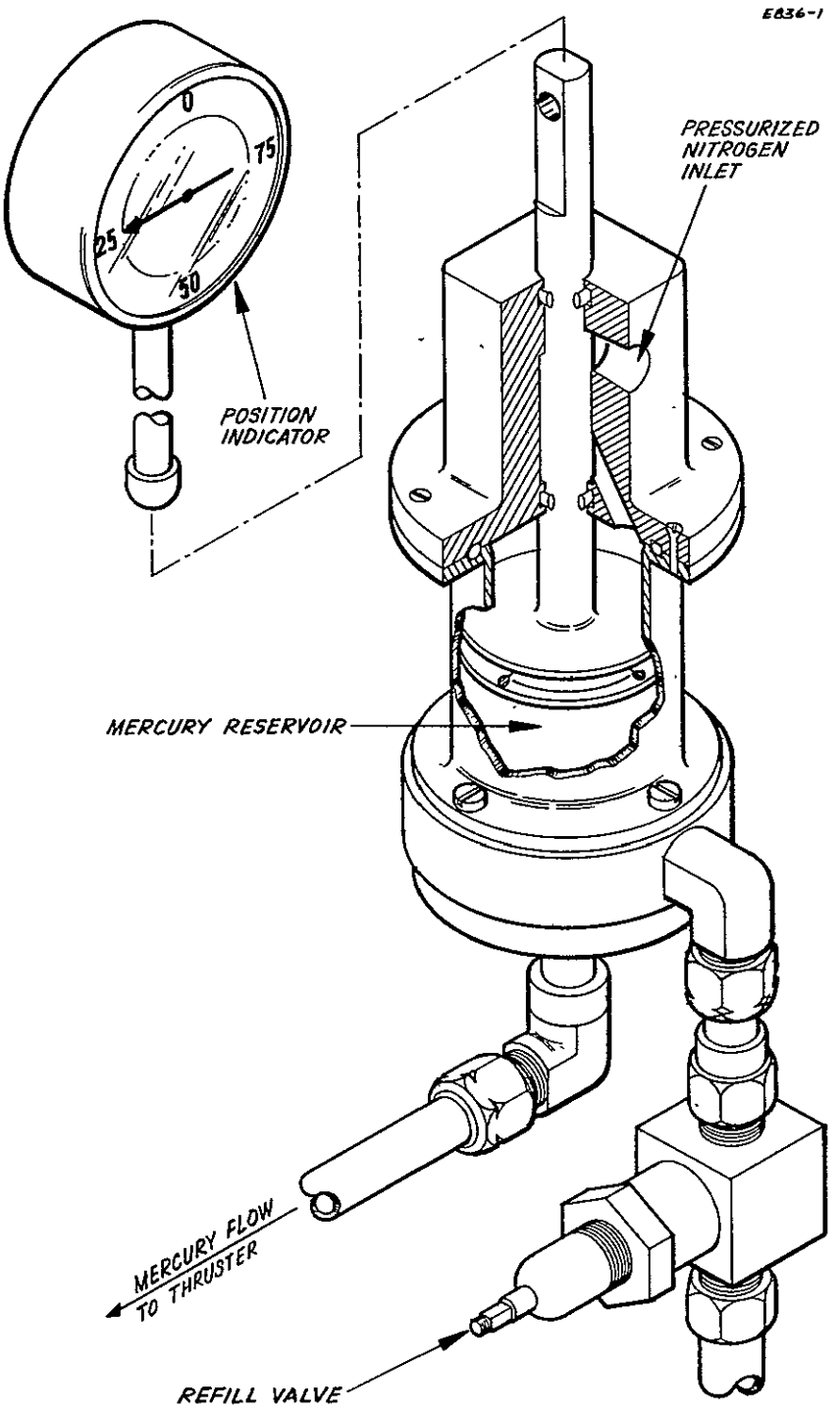

Fig. 5. Gas pressurized mercury reservoir.

SECTION III

THERMAL ANALYSIS

Detailed thermal analysis is required to establish accurate quantitative criteria for the design of a lightweight, thermally integrated LM cathode thruster. The first detailed analysis of an electron-bombardment thruster was undertaken at HRL under Contract JPL 952129, in which a thermal simulation of the ion-extraction system was carried out. Because of the limitations of that program, the simulation did not include the discharge chamber.

A complete thermal simulation of the thermally integrated LM cathode thruster is being undertaken as part of the present effort. This work involves the following tasks: (1) carry out a detailed thermal simulation of the discharge chamber of the LM cathode thruster; (2) combine the simulations of the discharge chamber and ion-extraction system; (3) compare the predictions of the thermal simulation with temperatures measured experimentally with the 30 cm thruster to improve the accuracy of thermal simulation; (4) use the improved simulation to develop a lightweight, effective thermal design for a 20 cm thermally integrated LM cathode thruster; and (5) correlate the calculated thermal data with temperatures measured on the new thermally integrated 20 cm thruster in order to evaluate the thermal design.

Computer program TAS-1B, which is being employed to simulate the discharge chamber, is a digital computer program which solves for the steady-state temperature distribution in a lumped parameter network of temperature points (nodes) and heat flow paths (resistors). A node is provided for each portion of the device being modeled which is at a uniform temperature. The network may contain up to 80 nodes, and each node may be connected to any or all of the others. Any two nodes may be connected by two resistors, one representing conduction and/or convection and the other representing infrared radiation. In addition to exchanging heat with other nodes, each node may receive radiation and/or a direct heat input (as from internal dissipation of electrical energy).

The inputs to TAS-1B which are required to model a device are the power inputs, nodal areas, radiant emissivities, radiation view factors, and thermal conductances. The power inputs are determined from physical considerations similar to those used in the theory developed by W. Knauer at HRL.[8] General relationships have been determined to facilitate calculation of the remaining quantities for a discharge-chamber model comprising 28 nodes. The generality of these relationships expedites thermal analysis over an entire range of geometrical variations of the thruster configuration. A small computer program has been written to automate this calculation.

The thermal profiles of the new 20 cm thruster and the existing 30 cm thruster have been calculated, and the 30 cm thruster has been instrumented for measurement of its temperature profile. The measured profile is in reasonable agreement with the results of initial computer calculations.

A. DISCHARGE CHAMBER HEAT DISTRIBUTION

A physical theory has recently been developed by W. Knauer for determining the limits of power efficiency of ion thruster discharges.[8] With only slight modifications, the same physical considerations have been used to determine the distribution of heat inputs to an LM cathode thruster which arise from discharge chamber losses.

The following general assumptions used by Knauer are assumed to be applicable to the LM cathode thruster:

1. The plasma is uniformly distributed within the discharge chamber.

2. The plasma electrons in the discharge chamber possess a Maxwellian energy distribution with a temperature T_p which is constant throughout the chamber.

3. The plasma potential in the discharge chamber is uniform at a value ΔV_A above the anode potential V_A, except for positive potential barriers and sheaths near walls.

4. The ion extraction screen is at cathode potential and permits passage of a fraction α of the arriving ions. The remaining fraction $(1 - \alpha)$ is neutralized upon impact, and re-enters the discharge in the upstream direction.

5. The endplate of the discharge chamber is at cathode potential and all impacting ions recombine and come off as neutrals.

In addition, for the LM cathode thruster it is specifically assumed that

6. A uniform plasma exists within the cathode-cup pole piece which has a potential V_C and a Maxwellian electron energy distribution of temperature T_C. Electrons leaving the cathode are thermalized in this region before being emitted as "primary" electrons into the main discharge-chamber plasma.

7. An amount of heat $P_{K,th} = I_K V_{K,th}$ is delivered directly to the cathode; $V_{K,th}$ is a measured quantity which has been shown to be independent of the cathode current I_K. Based on experimental evidence, it is assumed that an average electron loses an energy of $eV_{K,th}$ before actually emerging from the cathode.

8. Ions are prevented from reaching the anode. This assumption is based on the plasma-probe measurements (by Knauer, et al.,[9] in both hollow- and oxide-cathode thrusters and by Eckhardt, et al.,[10] in an LM cathode thruster) which indicate a small positive potential ridge near the anode which prevents the impingement of ions which originate at the center of the discharge chamber.

Employing these assumptions, the minimum total energy expenditure per beam ion $eV_S|_{min}$ in the discharge chamber of an electron-bombardment thruster has been shown by Knauer to be equal to

$$eV_S|_{min} = \frac{\beta\delta}{\eta_m} eV_A + \left(\frac{\delta}{\eta_m} - 1\right) eV_A. \qquad (1)$$

The terms introduced in this equation are defined below. The quantity

$$\beta = \frac{\text{minimum number of primary electrons}}{\text{ionization}} = \frac{\text{energy consumption per ionization}}{\text{maximum energy available from "primary" electron}}$$

or

$$\beta = \frac{eV_i + e\Delta V_A + \frac{3}{2}kT_p + \frac{1}{\overline{\nu}_i}\sum_n eV_n \overline{\nu}_n}{e(V_A - V_{K,th} - V_C) + \frac{3}{2}kT_C - \frac{3}{2}kT_p}$$

where V_i is the propellant ionization potential (for mercury $V_i = 10.4$ V), $\overline{\nu}_i$ is the ionization frequency averaged over the electron energy distribution, $\overline{\nu}_n$ is the averaged excitation frequency of atomic energy level n, due to collisions, eV_n is the energy of level n, and k is the Boltzmann constant.

The quantity

$$\delta = \frac{\text{number of ionizations}}{\text{atom}} = \epsilon \left(\frac{2}{\alpha} - 1\right)$$

where ϵ is the ionization probability of an atom making one transit across the discharge chamber and, as before, α is the transparency of the ion extraction system. Finally, the quantity

$$\eta_m = \text{mass utilization efficiency} = \frac{\text{number of beam ions}}{\text{atom}} =$$

In practice, the measured value of source energy per ion V_S will exceed the minimum value by some amount resulting from less-than-optimum confinement of "primary" electrons. Incomplete containment causes the average "primary" electrons to arrive at the anode with an energy ΔE above the minimum possible energy of $3/2\ kT_p$. Knauer's theory can be modified to include these additional losses by subtracting ΔE from the denominator in the expression for β and by including it in the calculation of the term $1/\nu_i \sum_n e\, v_n \bar{\nu}_n$ appearing in the numerator. Thus, for an LM cathode thruster which is not optimized to the fullest extent, a new value β' can be written as

$$\beta' \equiv \frac{eV_i + e\Delta V_A + \frac{3}{2} kT_p + \frac{1}{\bar{\nu}_i(\Delta E)} \sum_n eV_n \bar{\nu}_n (\Delta E)}{e(V_A - V_{K,th} - V_C) + \frac{3}{2} kT_C - \frac{3}{2} kT_p - \Delta E}$$

For experimentally measured values of the source energy per ion V_S, eq. (1) can now be modified as follows:

$$eV_S = \frac{\beta'\delta}{\eta_m} e V_A + \left(\frac{\delta}{\eta_m} - 1\right) e V_A. \qquad (2)$$

Equation (2) is then used to determine the quantity ΔE.

The distribution of heat input to the body of an LM cathode thruster can be evaluated using the terms of (2). The energy deposited directly in the cathode per beam ion E_{ν} is given by

$$E_K = \frac{V_{K,th}\ I_K}{I_B}$$

where I_B is the ion beam current. The energy per beam ion deposited in the cathode-cup structure E_C is equal to the energy going into the cathode-cup plasma minus that which is transported into the main discharge, or

$$E_C = \frac{\beta'\delta}{\eta_m} \left(eV_C - \frac{3}{2}\ kT_C \right)$$

The energy per beam ion expended at cathode-potential walls E_W can be written as the number of wall recombinations per beam ion times the sum of the potential energies gained by the recombining ion, or

$$E_W = e \left(\frac{\delta - \eta_m}{\eta_m} \right) \left(V_A + \Delta V_A + V_i \right)$$

The energy deposited in the anode per beam ion E_A is equal to the sum of the energy deposited by "primary" electrons and that deposited by electrons which result from the creation of plasma ions, or

$$E_A = \frac{\beta'\delta}{\eta_m}\ \Delta E + \left(\frac{\beta'\delta}{\eta_m} + \frac{\delta}{\eta_m} \right)\ \frac{3}{2}\ kT_p^{*}.$$

The excitation energy per beam ion E_ν is distributed uniformly throughout the interior of the discharge chamber and is given by

$$E_\nu = \frac{\delta}{\eta_m} \left(\frac{1}{\overline{\nu_i}(\Delta E)} \cdot \sum_n \overline{\nu_n}(\Delta E)\ eV_n \right)$$

The sum of these energies and the energy of dissociation per beam ion V_i must equal the source energy per ion V_S.

*The influence of the anode work function has not been included in this treatment; it will be included in future calculations.

Using these expressions; typical values of the heat inputs have been calculated for the 30 cm thermally integrated LM cathode thruster. The thruster parameters listed below are typical for operation of the 30 cm thruster.

Beam current I_B	=	1110 mA
Mercury flowrate equivalent I_a	=	1360 mA
Discharge current I_K	=	7 A
Discharge voltage V_A	=	45 V
Source energy per ion V_S	=	283 eV/ion
Mass utilization efficiency η_m	=	83%

The cathode used to obtain the above data is similar to LM cathode K-25-V, for which the specific thermal load $V_{K,th}$ = 4 W/A (Ref. 1); this value is used in the following calculations. Plasma potential and electron temperature have been measured previously for an LM cathode thruster.[10] Although the thruster employed for those measurements was less efficient than the 30 cm thruster, the following data are assumed to be applicable to the present case.

Discharge chamber plasma temperature T_p	=	7.8 eV
Cathode-cup plasma temperature T_C	=	3 eV
Cathode-cup plasma potential V_C	=	10.7 V
Anode sheath potential ΔV_A	=	5 V

The transparency of the ion-extraction system is assumed to be equal to the transmission of the screen electrode, so that $\alpha = 0.7$. For this preliminary calculation the excitation energy per beam ion is assumed to be given by $E_\nu = (eV_i)\ \delta/\eta_m$, which is independent of ΔE. For mercury, the ionization potential V_i = 10.4 V. From these data, the energy of an average primary electron upon arrival at the anode is calculated to be ΔE = 10.3 eV. The number of primary electrons per ionization β' = 2.93 and the ratio δ/η_m = 1.86. Using these values, the discharge-chamber heat inputs per beam ion are calculated to be

E_K = 25 eV/ion

E_C = 34 eV/ion

E_W = 52 eV/ion

E_A = 142 eV/ion

E_ν = 20 eV/ion

The summation of these energies plus the dissociation energy per beam ion, eV = 10.4/ion, is equal to the source energy per ion V_S = 283 eV/ion.

These values of heat input to the various electrodes serve as the required power inputs to the computerized thermal simulation of the discharge chamber.

B. COMPUTER SIMULATION

The geometrical configuration of nodes which is utilized to describe the thermal characteristics of the LM cathode thruster must be sufficiently similar to the actual thruster design to provide an accurate simulation, yet simple enough to provide a tractable theoretical problem. Figure 6 illustrates the system of nodes which is used to model the thermal properties of the thruster geometry illustrated in Fig. 1. Nodes 1 to 28 represent the discharge chamber and its ground-screen shroud, nodes 29 to 49 represent the ion-extraction system studied previously under Contract JPL 952129, and nodes 50 to 52 simulate the thruster environment. The generalized dimensions of the model are shown in Fig. 7. This model includes the necessary generality for the investigation of the dependence of the thruster thermal properties on the design variables in order to obtain an optimum configuration. The problem is made more readily tractable by employing a number of assumptions. In modeling the discharge chamber it is assumed that the cathode-cup pole piece and propellant distributor baffle can be neglected in the configuration of nodes. Their influence can be taken into account by the appropriate calculated heat inputs to be discussed later. The anode connector is assumed to have the same outer diameter as the body of the thruster and to conduct a small quantity of heat to the body. The associated thermal conductance is assumed to be equal to that calculated for the thin stainless steel wall through which the anode-connector studs pass. This assumption is based on the supposition that the stainless steel wall is in good thermal contact, through radiation transfer, with the front section of the anode and anode connector. It is also assumed that the ground screen has a fractional open area of f_s and that it lies very close to the thruster body. The influence of multiple heat shields (e.g., between the thruster walls and the anode) is taken into account through calculated effective emissivity ϵ_e given by

$$\epsilon_e = \frac{2\epsilon}{(2 - \epsilon)(n + 1) + \epsilon}$$

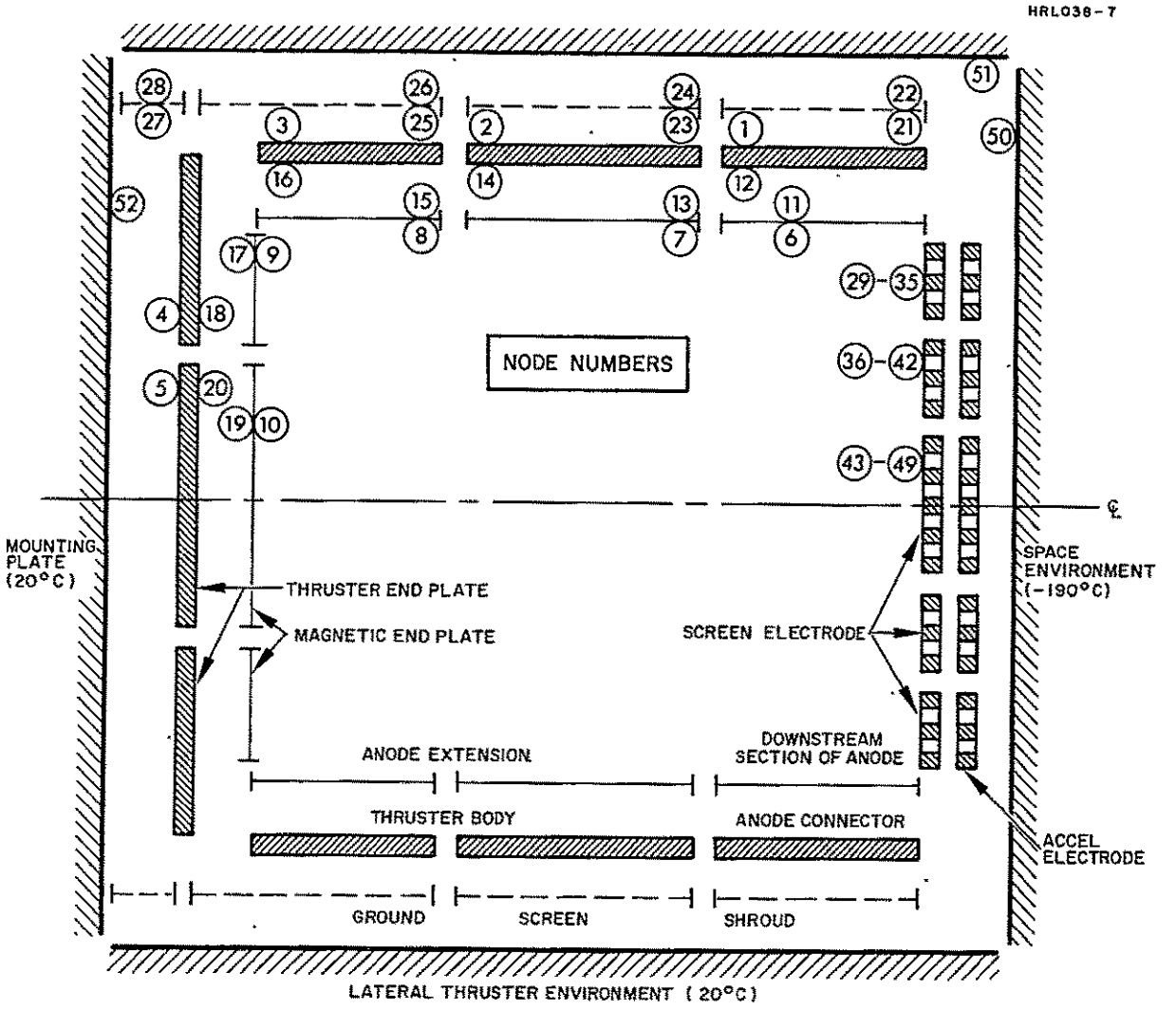

Fig. 6. Configuration of nodes used to simulate the thermal characteristics of an LM cathode thruster. The numbering of nodes is indicated in the upper half of the schematic.

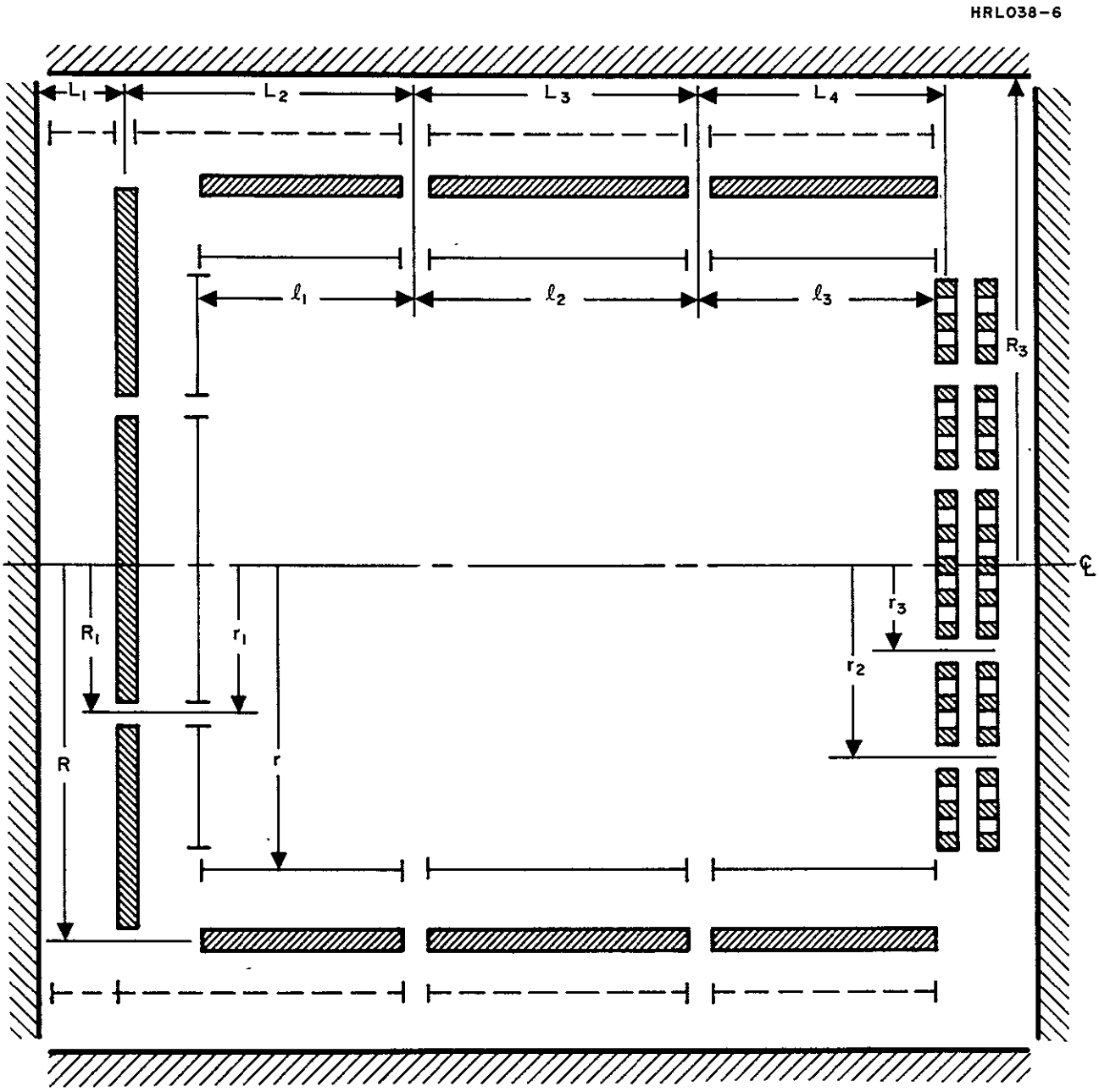

Fig. 7. Generalized dimensions of the model used to describe the LM cathode thruster.

where ϵ is the actual emissivity of one of the heat-shield surfaces (all involved surfaces are assumed to have the same emissivity) and n is the number of heat shields.

The method of modeling the ion-extraction system was described in Ref. 11. Under Contract JPL 952129 the extraction system was divided into three concentric rings, as shown in Fig. 6. There is no thermal conduction between screen and accel electrodes and only directly opposed rings are assumed to be coupled by radiation. The adjacent rings of any one electrode are coupled by conduction. Associated with each of the three rings are seven nodes, as illustrated in Fig. 8.

The thruster environment has been simulated in a manner which will allow the investigation of a number of possible situations. Node 50 represents the space environment, which has a fixed temperature and an emissivity of one. Node 51 also represents the space environment when the lateral surfaces of the thruster are exposed to space, but it can simulate the environment of a density packed thruster array when its emissivity is set at zero. Node 52 can be made to represent an adiabatic wall when its emissivity is set at zero, or it can absorb radiation when a non-zero emissivity is used.

Calculation of the nodal areas, thermal conductances, and view factors for radiation transfer between each node and all other nodes is tedious but straightforward. The procedure is illustrated in Ref. 11. General relationships for the various quantities have been derived and a small computer program has been written which is employed to calculate values for any given dimensions and thermal conductivities. These quantities, along with the emissivities, heat inputs, and temperatures of fixed temperature nodes, constitute the inputs for computer program TAS-1B. The results for two specific cases analyzed to data are given below.

1. 20 cm Thruster

Figure 9 illustrates the thermal model of the new 20 cm thermally integrated LM cathode thruster illustrated in Fig. 1. The heat inputs, which are assumed to be similar to those experienced with the 30 cm thruster, are determined from the calculations of Section III-A, with the following added assumptions: (1) the ion beam current I_B = 1.0 A; (2) half of the heat deposited in the cathode cup E_C goes to the cathode heat shield and the remainder is distributed uniformly throughout the interior of the discharge chamber; (3) the heat deposited in walls which reside at cathode potential is distributed to the representative nodes in proportion to their area; (4) all anode power E_A is deposited in the downstream third of the anode; (5) the power going into atomic excitations is redistributed uniformly to the interior of the discharge chamber. It is also assumed that 5 W of magnet power is deposited, in proportion to area, in the exterior of the thruster body and anode connector, and that 1% of the ion beam power is deposited in nodes 39 and 46.

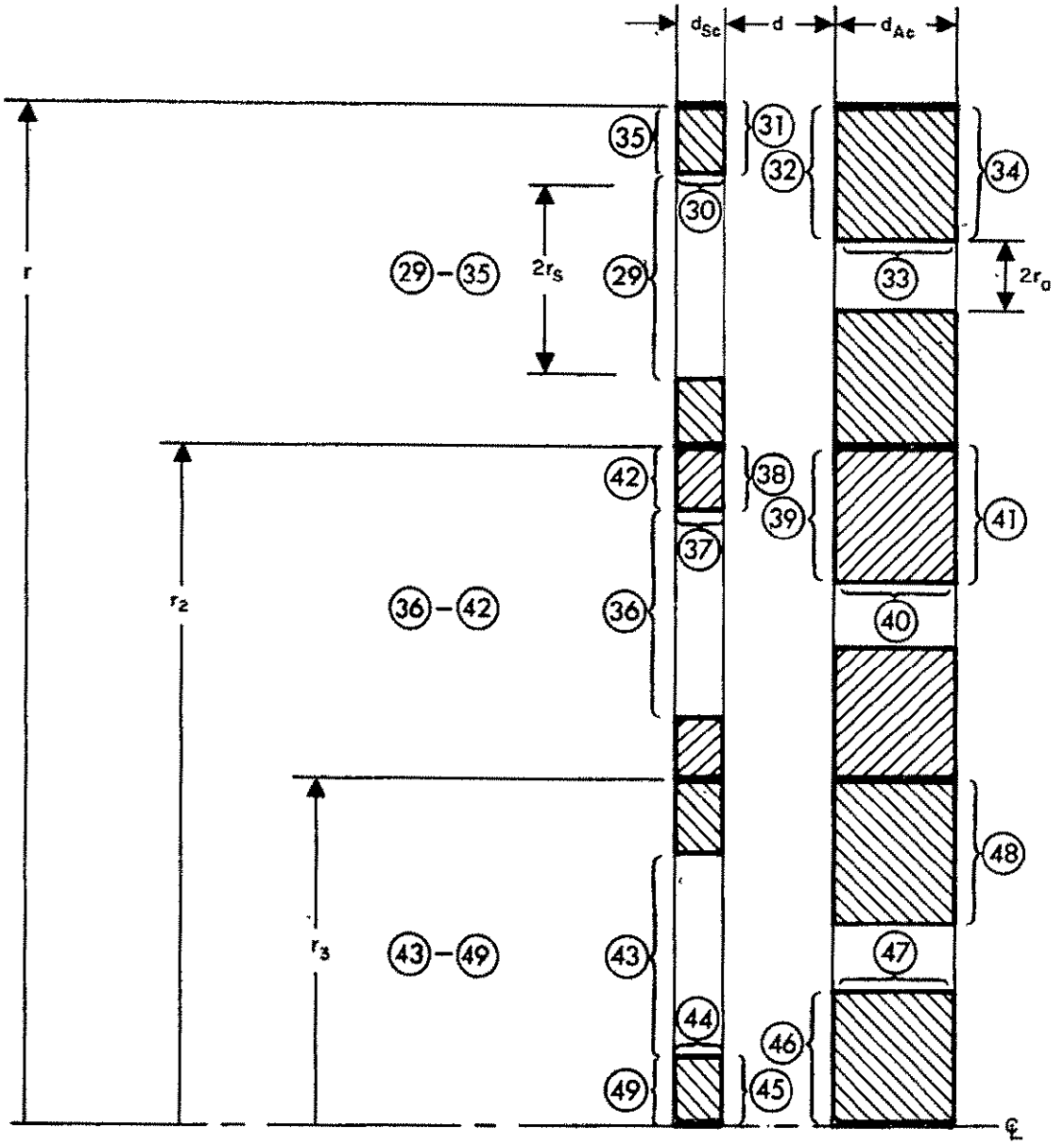

Fig. 8. Configuration of nodes used to simulate the thermal characteristics of the ion-extraction system.

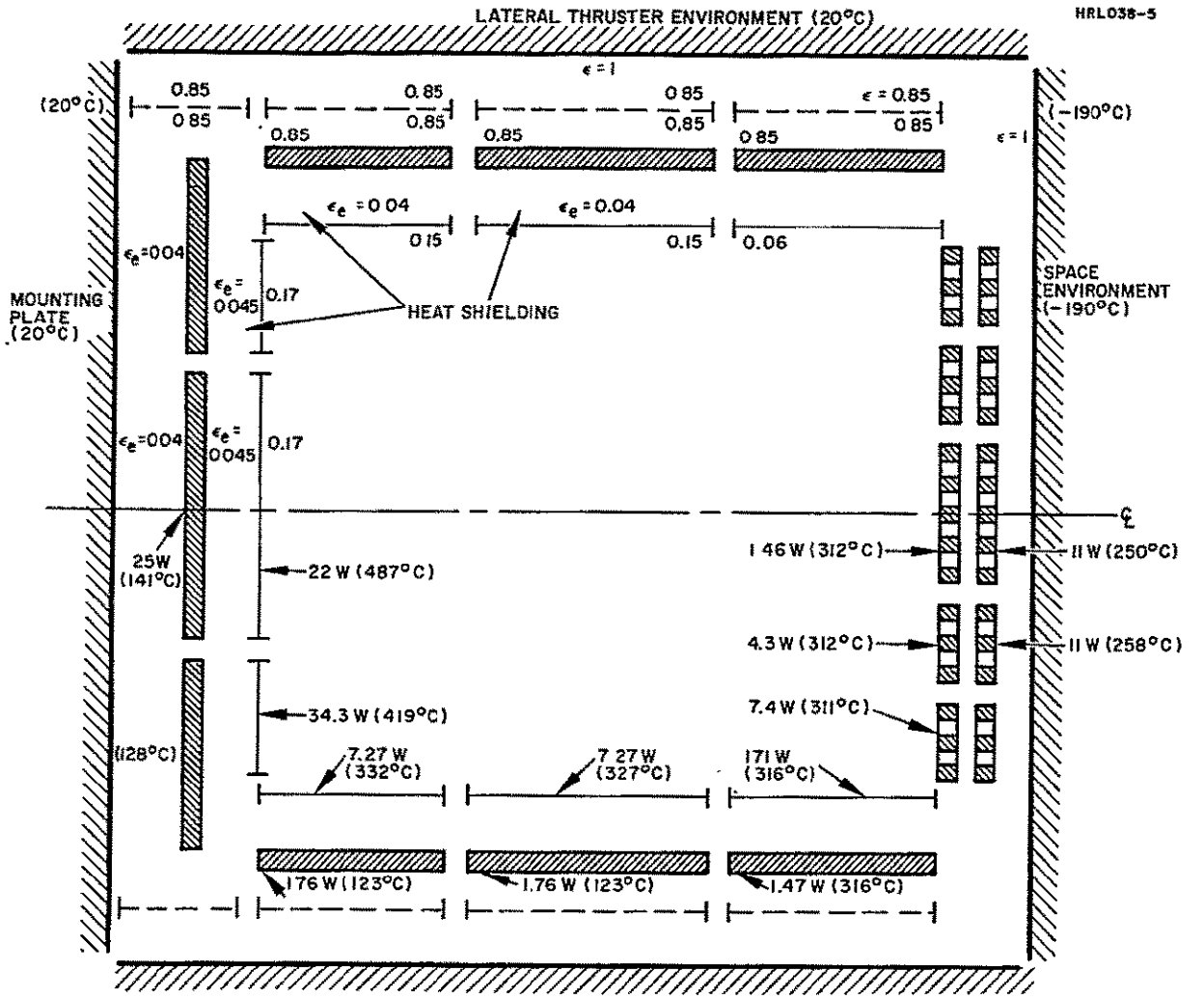

Fig. 9. Thermal model of the 20 cm thermally integrated LM cathode thruster. The assumed emissivities and temperatures of fixed-temperature walls are noted in the upper half of the schematic. The heat inputs and resultant temperature distribution are indicated in the lower portion of the diagram.

The emissivities of the various surfaces are assumed to have the values given in Fig. 9. The outer surfaces of the thruster body are assumed to be painted with a high emissivity paint, and the values of the remaining emissivities are best estimates for the materials and surface conditions expected for the 20 cm thruster.[12] Three heat shields are assumed to be added between the thruster endplate and the magnetic endplate, and between the thruster body and the anode extension. Two heat shields are included between the thruster endplate and the mounting plate in order to simulate the effect of the feed system assembly which will be mounted in this region. The resultant effective emissivities have been calculated and are noted in Fig. 9. The temperatures of the fixed temperature nodes 50-52 are given in Fig. 6. Node 51 is set at 20°C to represent the water cooled shroud employed in vacuum chamber experimentation. The dimensions used in the calculations are appropriate for the new 20 cm thruster.

The resulting temperature profile is given in Fig. 9. The temperature of the node (node 5) which contains the cathode is well within the range over which efficient and reliable operation is achieved with the LM cathode.

2. 30 cm Thruster

Figure 10 illustrates the thermal model of the existing 30 cm thermally integrated LM cathode thruster. (It should be noted that a ground screen is not employed in the existing configuration.) The heat inputs are determined from the results of Section III-A, with the same added assumptions (1) to (5) used previously with the 20 cm thruster. It is also assumed that 12 W of magnet power is deposited, in proportion to area, to the exterior of thruster body and anode connector, and that 1% of the ion beam power is deposited in nodes 39 and 46. The values of the emissivities are best estimates for the materials and actual surface condition of the 30 cm thruster.[12] Two heat shields are included on the discharge-chamber side of the thruster endplate to represent the magnetic endplate.

The resulting temperature profile, illustrated in Fig. 10, is compared with experimental data in the following section.

C. TEMPERATURE MEASUREMENTS

The temperature distribution achieved during operation of the 30 cm thruster has been determined from thermocouple measurements. The thermocouple outputs were monitored on an International Instruments millivolt meter to obtain temperature data accurate to within ±1°C. At a

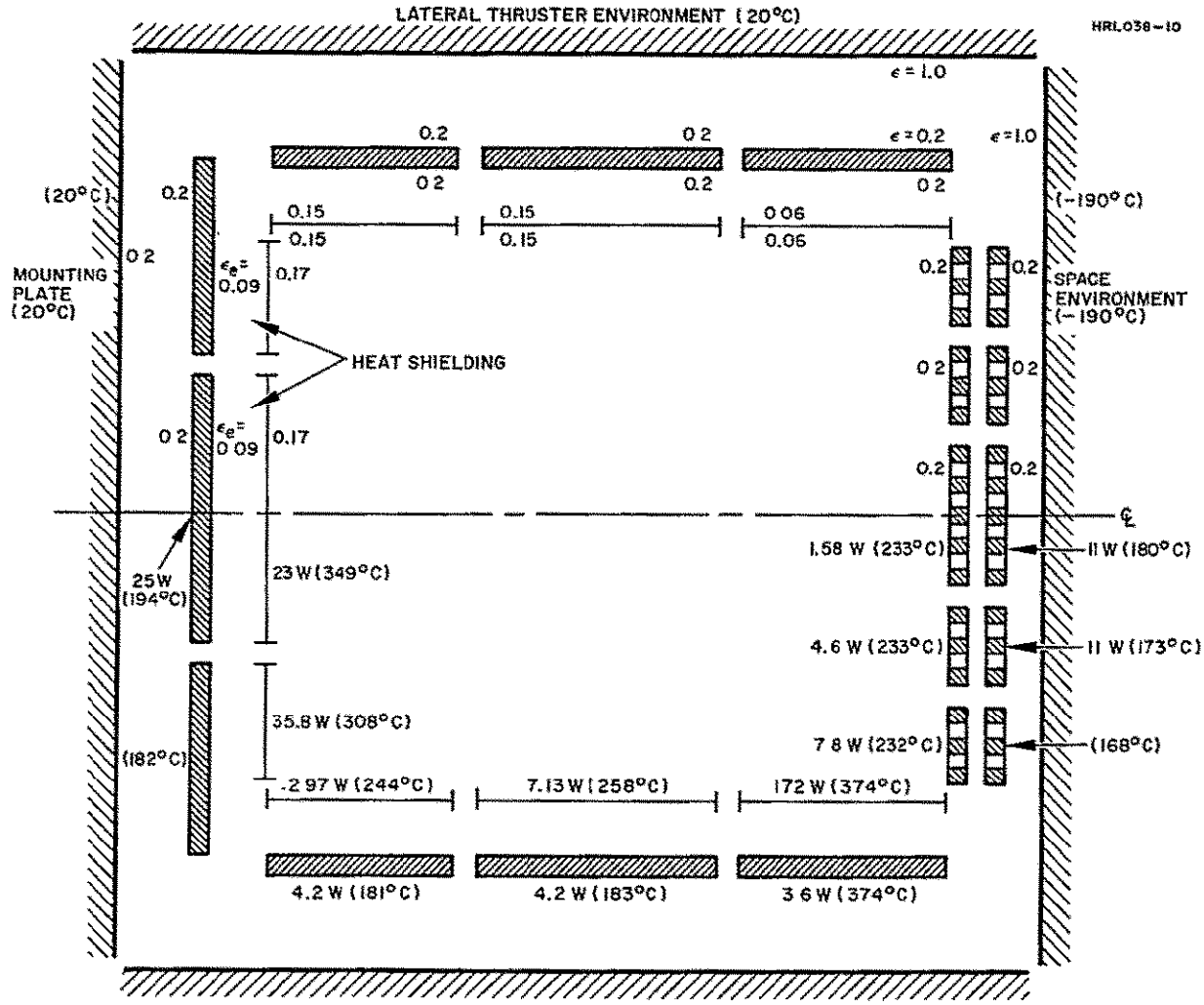

Fig. 10. Thermal model of the 30 cm thermally integrated LM cathode thruster. The assumed emissivities and temperatures of fixed-temperature walls are noted in the upper half of the schematic. The heat inputs and resultant temperature distribution are indicated in the lower portion of the diagram.

beam current I_B = 1.1 A, all external surfaces of the thruster operated at less than 200°C, except for the external anode connector which reached a temperature of 281°C. The downstream aluminum section of the anode itself reached a temperature of only 292°C, which demonstrates close thermal coupling with the external connector. The thin stainless-steel anode extension achieved a uniform temperature within 2°C of the downstream section.

The initial theoretical temperature profile obtained for the 30 cm thruster and illustrated in Fig. 10 corresponds generally with these data. This correspondence confirms the theoretically based assumption that the greatest portion of discharge heat is deposited on the downstream section of the anode, and thus justifies the basic criteria which determine the thermal designs of both the 20 cm and 30 cm thrusters.

SECTION IV

COMPONENT DEVELOPMENT

A. 20 cm THRUSTER

The present effort is directed toward design and construction of a thermally integrated 20 cm LM cathode thruster optimized for operation at beam currents I_B = 0.5 A to 1.0 A. The discharge-chamber design is derived from the configuration of an existing 20 cm LM cathode thruster, which uses an externally cooled LM cathode. During the third quarter of the current contract, this thruster was optimized for operation at a beam current $I_B \approx 600$ mA (Ref. 5). At a beam voltage V_B = 2 kV, the total source energy per ion was V_S = 266 eV/ion, at a mass utilization efficiency η_m = 80%. Efforts are now being made to reoptimize this 20 cm thruster at beam currents in the range 0.5 A to 1.0 A, in order to determine in advance the techniques required for optimizing the thruster which is now under construction. The configuration which is found to yield optimum performance with the present thruster will be employed as the initial configuration for the 20 cm thermally integrated LM cathode thruster. Approaches to achieving the desired results are based on the optimization undertaken previously with the 30 cm thermally integrated LM cathode thruster under the first phase of this contract.[1] On this basis, the 20 cm thruster was modified (as shown in Fig. 11) to operate with single-capillary fed LM cathode K-51, mounted on the nitrogen-cooled aluminum plate which is shown in Fig. 12. A cathode-cup pole piece was installed which has a wall thickness of 0.051 cm and sixteen 0.79 cm diameter holes in two rows around its periphery. The holes were covered with stainless steel mesh and their transmission could be varied by use of a movable shutter. The position of the shutter determined, in part, the fraction of the neutral mercury flow which emerged from the open end of the cathode-cup pole piece. The baffle, which also influenced the distribution of neutral mercury in the discharge chamber, was the same movable zone baffle used in the previous 20 cm thruster optimization program. It consisted of an annular disk with an inner diameter approximately equal to that of the cathode-cup pole piece and an outer diameter equal to half the diameter of the thruster anode, and a coplanar central disk with a diameter 0.290 cm less than the inner diameter of the cathode-cup pole piece.

In initial experiments with the 20 cm thruster, a beam current I_B = 1.0 A was achieved at a beam voltage V_B = 2 kV; at a total source energy per ion V_S = 430 eV/ion the mass utilization efficiency

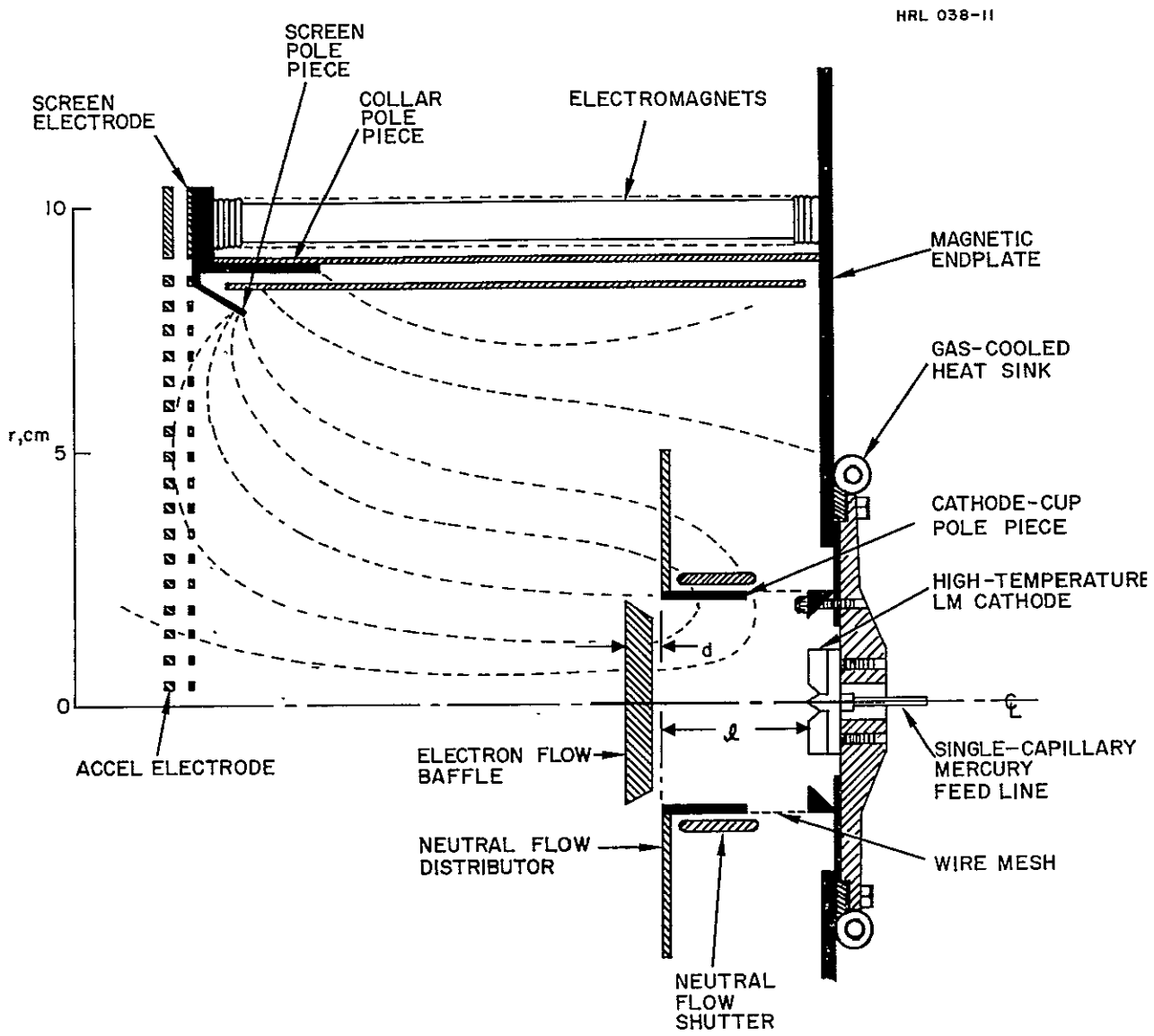

Fig. 11. The 20 cm thruster operated with an externally cooled LM cathode.

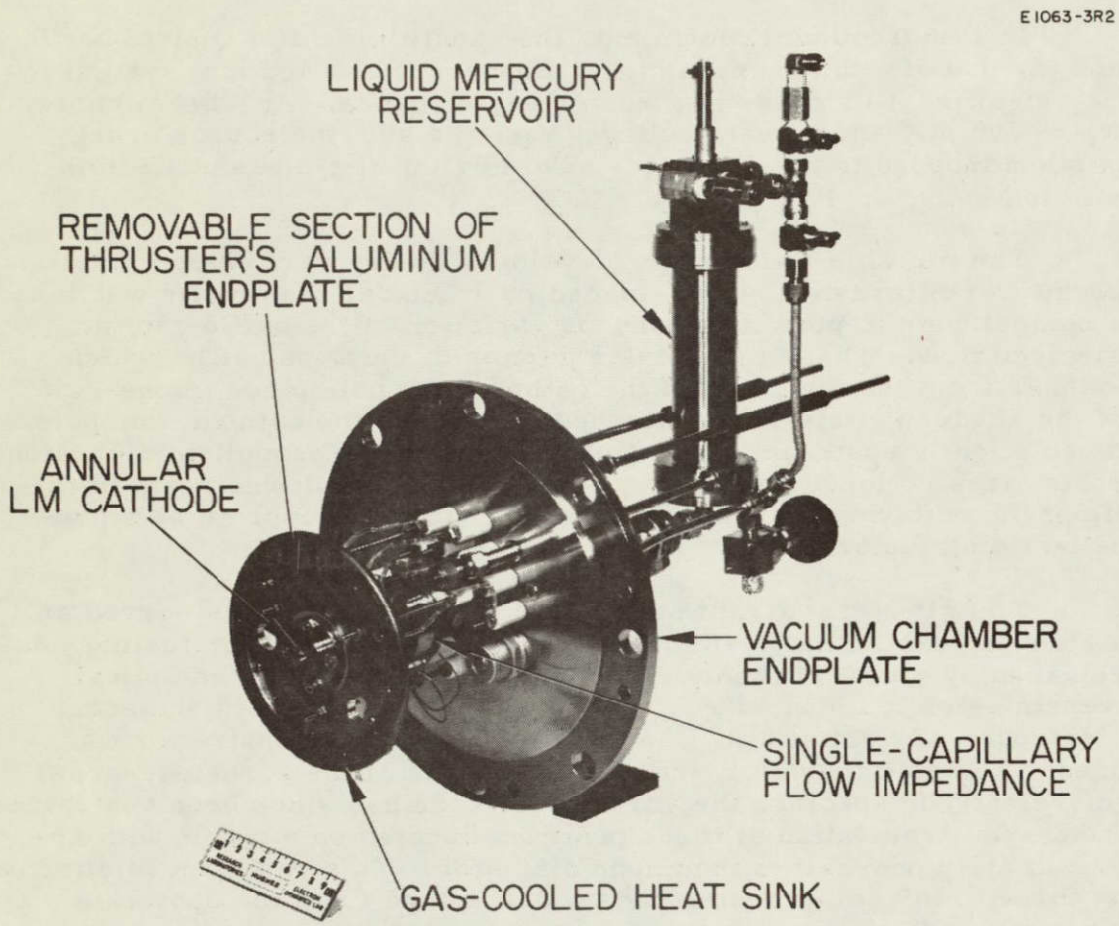

Fig. 12. Photograph of single-capillary-fed LM cathode K-51 provided with a gas-cooled heat sink.

was η_m = 85%. These data were obtained without using the beam constrictor which had previously been employed for operation of the 20 cm LM cathode thruster.

In a subsequent experiment, the substitution of a conical baffle and the use of a thin-screen high-transparency ion-optical system led to a significant increase in thruster performance. At a beam current I_B = 790 mA and a beam voltage V_B = 2 kV, the source energy per ion dropped to a value V_S = 290 eV/ion at a mass utilization efficiency η_m = 88%.

The movable zone baffle, developed during earlier optimization of the 20 cm thruster, was replaced by a central-disk baffle which had a conical edge to permit continuous variation of the baffle gap for electron flow. The outer annular portion of the zone baffle (which extends from the diameter of the cathode-cup pole piece to one-half of the anode diameter) was attached directly to the cathode-cup pole piece slightly upstream of the lip; with the use of propellant diversion ports, it is no longer necessary that it be located downstream of the lip of the cathode-cup pole piece in order for it to operate as a propellant distributor.

The 51% transparent ion-optical system, which has served as a standard extraction system for previous 20 cm thruster testing, was replaced by a thin-screen (0.076 cm thick) system with an optical transmission of about 71%. The spacing between screen and accel electrodes was set at 0.127 cm and again no beam constrictor was used. To avoid thermally induced variations of the screen-to-accel interelectrode spacing, the screen electrode has since been restrained from axial translation at three positions located on a circle with approximately one-half of the anode diameter. This restraint is effected by three 0.159 cm diameter rods which extend from the upstream end plate of the discharge chamber. Each rod is attached to the screen electrode by a bolt and two nuts which obscure only one of the beam-forming apertures.

B. LIQUID MERCURY FEED SYSTEM

A liquid-mercury feed system is now being constructed from components developed during the earlier phase of this contract[1] and under Contract NAS 7-539 (Ref. 13). The only new component being developed under the current phase of this contract is a liquid-mercury flowmeter which measures the instantaneous value of the mercury flowrate equivalent over the range from I_a = 0.5 A to 1.0 A.

1. Electromagnetic Pump

An improved electromagnetic (EM) pump has been built which utilizes O-ring seals between a nylon pump body and the current-carrying electrodes, the magnetic pole pieces, and the mercury feed channels (see Fig. 13). Nylon with 20% glass reinforcing has been employed because of its high strength, high service temperature, and low coefficient of thermal expansion, which makes it more compatible with the thruster operating environment. Operation of the pump is similar to that of the design developed under Contract NAS 7-539 (Ref. 13), except that problems of leakage have now been eliminated.

The over-all dimensions of the pump are 8.5 cm x 6.5 cm x 3.5 cm and its weight is 301 g. The maximum field is 9 kG in a narrow pumping region which is 0.025 cm wide and 1.27 cm square; the pump is designed so that the magnetic field is concentrated in the pumping region. Narrow channels are cut into the nylon pump body between the pumping region and the mercury feed line in order to discourage potential eddy currents in the mercury flow. The pole pieces have been coated with a thin layer of teflon (0.003 cm thick) which is sprayed and baked onto the surface to provide electrical insulation from the mercury.

The electrodes which contact the liquid mercury are slotted to increase their surface area. The electrodes operated under Contract NAS 7-539 were plated with platinum so that they would be wetted by the mercury. Both features were incorporated to reduce the electrical resistance of the contact surface between the mercury and the electrode surface. The platinum-plated electrodes performed satisfactorily throughout the testing of the prototype device under Contract NAS 7-539. After one year of storage and intermittent use, this pump was disassembled for inspection under the current contract. Although no degradation in performance was observed either before or after that time, some pitting of the platinum-plated surface was noted. Thus there is some apprehension concerning the long term integrity of a platinum surface under possible attack by mercury.

A research and development effort is now under way under the current contract which will either determine that the platinum surface is resistant to attack by mercury or locate a more suitable substitute material for use as an electrode material. For the first performance test, the pump was fitted with nonwetting, stainless steel electrodes. The initial pump configuration included two permanent magnets to provide a magnetic field intensity of 12 kG in the narrow pumping region. In direct correspondence with design expectations, the pump produced a static pressure head of 1.0 atm at 25 A, with a linear pressure-current function in the range from 0 to 1.0 atm. In a subsequent test,

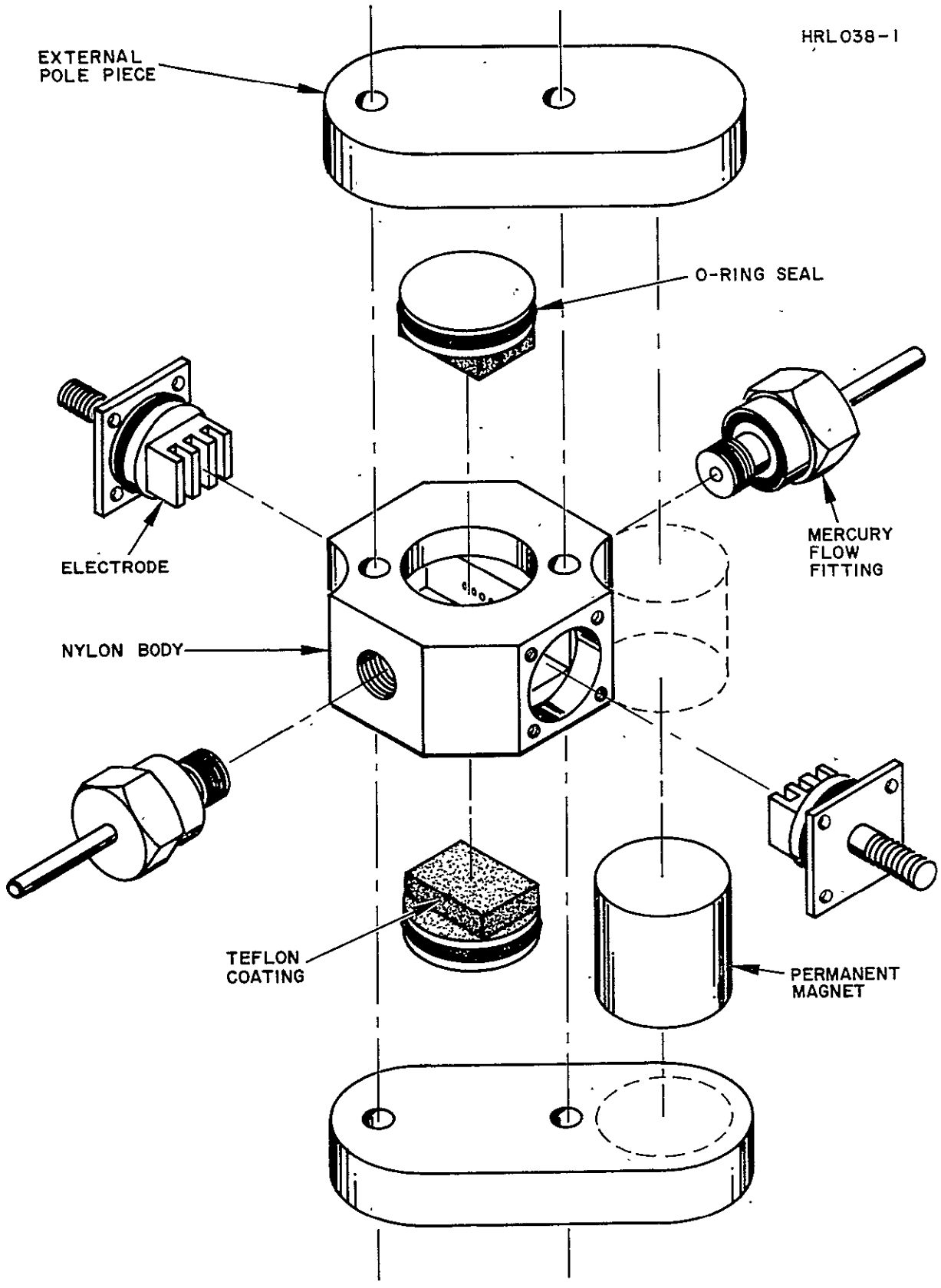

Fig. 13. Electromagnetic pump.

one of the two permanent magnets was removed and the pressure-current function was remeasured. The pump produced a pressure head of 0.75 atm at 25 A, or 75% the value obtained when both magnets were used. Removal of the one magnet reduced the pump weight 301 g, a 35% weight reduction from the initial configuration

Replacing the stainless steel electrodes in the EM pump with an otherwise identical set of molybdenum electrodes resulted in a marked decrease in power expenditure, while preserving essential the same pumping characteristics in terms of flow capacity and pressure-rise per ampere. As before, the pump generated a pressure head of 0.6 atm when driven at 20 A. However, the required power dropped from 20 W with the stainless steel electrodes to as low as 1.6 W with the molybdenum electrodes. This reduction is related to the superior mercury-wetting characteristics of the molybdenum surface which decreases the voltage drop across the pump to the value imposed by the resistance of the mercury itself.

The EM pump with molybdenum electrodes has undergone an 800 hour life test at 20 A electrical current, while circulating mercury in a vacuum environment. With the mercury flow set at an equivalent rate of approximately 3000 A, a total of 2,400,000 A-hours of mercury flow equivalent was circulated through the pump during the test. During the first 450,000 A-hours, the voltage drop across the pump rose steadily from 0.08 V to 0.16 V. The pump was disassembled at this time and the electrodes were removed, cleaned with soap cleanser, and replaced. The voltage across the pump dropped immediately to the previous low value. During the next 1,000,000 A-hours, the voltage slowly rose again, leveling-off finally at a value of slightly less than 0.5 V. After reaching this maximum value, the voltage drop across the pump began to decrease slowly throughout the duration of the test. When the test was terminated the voltage drop had decreased to 0.35 V. Further study will be required to determine the exact nature of the conditioning process which is associated with the voltage drop across the pump.

2. Mercury Flowmeter

Under the first phase of this contract, the mercury flowrate through a single-capillary flow impedance was shown to be a linear function of the pressure drop across its length.[1] This characteristic is exploited under the present effort by the development of a mercury flowmeter which utilizes a differential pressure transducer to measure the pressure drop across a calibrated section of the capillary flow impedance. A Winsco Model PB415 differential pressure transducer was used which yields a 25 mV signal output for an applied pressure

difference of 10 psi. The transducer output is linear to within 1% of full scale. This transducer measures the pressure drop across a single-capillary flow impedance, designated SC-5, consisting of a 915 cm length of 0.0178 cm (i.e., type 304 stainless steel tubing). Impedance SC-5 is attached to the upstream end of single-capillary flow impedance SC-3 (1,060 cm length of 0.014 cm i.e., type 304 stainless steel tubing) which simulates the flow impedance leading to an LM cathode.

The flowmeter has been calibrated by correlating the electrical output signal of the pressure transducer with the mercury flowrate which is determined by the rate of displacement of the piston of a gas-pressurized mercury reservoir. Data points were acquired at a rate of only one or two per day to insure that each value of the mercury flow rate would be determined to the same high accuracy anticipated from this instrument. The initial first ten data points confirmed the high expectations held for the flowmeter, exhibiting a linear output characteristic with a signal amplitude of 24 mV/A equivalent of mercury flow within a standard deviation of ±1% over the range from 0.2 A to 1.2 A. The first ten data points are indicated as solid circles in Fig. 14. The next seven data points, indicated as open circles, showed a marked increase in scatter as the calibration characteristic underwent a change to a new value which is described by the next 17 data points, indicated by solid triangles. The new calibration characteristic is also linear with an output signal of 24 mV/A equivalent with a standard deviation of slightly greater than ±1%, but it now exhibits a different intercept of transducer output for zero flow rate; whereas initially the pressure drop across capillary SC-5 approached a value 1.7 psi for zero flow rate, the value of the intercept shifted in time to a value of 2.5 psi. The reason for this shift in intercept and, in fact, for the existence of a nonzero intercept in the first place is discussed in the appendix. The existence of a nonzero intercept is believed to indicate the presence of minute gas bubbles which are lodged within the liquid mercury feed system. If these gas bubbles were not present, the pressure drop across capillary SC-5 would approach zero for zero flow rate, and no fluctuations could occur. Therefore, in order to eliminate time variations in the flowmeter calibration, even more stringent precautions than have been taken in the past[1] must be enforced to assure complete outgassing of both the feed system and the mercury liquid itself

3. Hydrogen-Bubble High-Voltage Isolator

The LM cathode thruster is isolated from the mercury storage reservoir by the use of a hydrogen-bubble high-voltage isolator. In this device, a small hydrogen bubble is introduced into the mercury flow stream within an insulated tube. Previous efforts with a

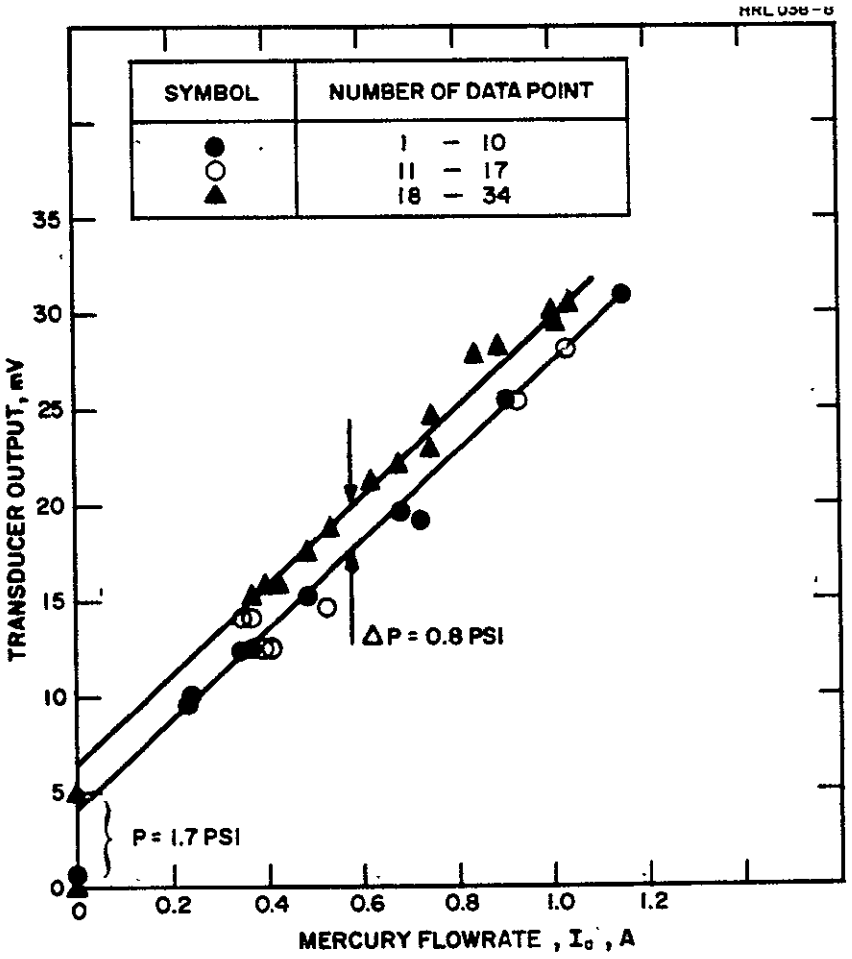

Fig. 14. Mercury flowmeter calibration characteristic.

hydrogen-bubble isolator utilized a teflon insulating tube.[1,13] With this design it was observed that the bubble decreased in length as it passed through the insulated section of the tube. An initial requirement for a new isolator design was to determine the cause of hydrogen loss.

An experiment was conducted to determine whether the hydrogen gas was being absorbed by the liquid-mercury column or was diffusing through the wall of the insulating teflon tube. The experimental apparatus consists of a glass U-tube with an inside diameter of 0.18 cm. One end of the tube was open and the other was fitted with a stainless steel valve. The tube was partially filled with mercury and the region between the mercury and the valve was pressurized with hydrogen until a pressure head of approximately 80 Torr was established. By measuring the rate of decrease in the volumn of the trapped hydrogen bubble, the absorption of hydrogen through the exposed surface of the mercury was determined to be less than 5×10^{-3} $cm^3/hour/cm^2$. The same type of apparatus was then fitted with a length of teflon tubing between the mercury and the stainless steel valve. The rate of hydrogen diffusion through the teflon tubing was much greater than absorption by the mercury. Alumina tubing was also tested. The experimental results of all the tests are shown in Table III; the results are expressed as the volumetric leak rate of hydrogen per unit area exposed to the tested media (i.e., glass, teflon, alumina).

TABLE III

Results of H_2 Diffusion-Absorption Test

Test Material	Leakage Rate, $cm^3/hour/cm^2$
Mercury (contained in a glass tube)	0.0045
Teflon (tube section with a 0.078 cm wall thickness)	0.42
Thermo-plastic teflon (tube section with a 0.038 cm wall thickness)	0.028
Alumina (tube section with a 0.078 cm wall thickness)	0.00003

Hydrogen diffuses through a unit area of the teflon tubing 6 to 100 times more rapidly than it is absorbed by the mercury. Because the surface area of teflon exposed to the gas is approximately 20 times greater than that exposed to the mercury, it is concluded that thin-wall teflon tubing is not acceptable for the insulated tube. Glass is presently being considered as an interim material for the tube while a cast ceramic body with the proper flow passage is being developed. Work in this area is progressing steadily, and a casting is scheduled to be delivered soon for evaluation.

A palladium diffuser assembly has been completed and tests to determine its operating characteristics have begun. Palladium was used instead of iron as the diffuser element because of its inherent characteristic of passing the hydrogen gas at a lower temperature. If the diffuser is operated at 250°C (50°C above thruster ambient), the flow rate can be controlled with minimum power expenditure.

Design of the HV isolator is complete and construction is 85% finished. The design incorporates fittings which allow interchangeability of alternative insulating tube sections and pressure reservoirs. This design utilizes a commercial high-pressure reservoir for hydrogen gas storage which is heavy and bulky. An alternative reservoir design has been completed which is 70% lighter than the commercial reservoir. The new design features welded joints, lightweight input and output terminations, and circular construction for a better fit into the feed system package. Parts for this reservoir are presently being fabricated in the machine shop, and the reservoir will be integrated into the thruster feed system upon completion.

SECTION V

CONCLUSIONS

Fabrication of the 20 cm LM cathode thruster system is nearing completion. Modifications of the discharge chamber which will be required for efficient operation at a beam current I_B = 0.5 A to 1.0 A are being anticipated by optimization of a 20 cm thruster which employs an externally cooled LM cathode. In a concurrent effort, a lightweight LM cathode has been constructed and elements for assembly of a liquid-mercury feed system are being developed. Although the thruster and its liquid-mercury feed system are characteristically enclosed within a ground-screen shroud, provision has been made to allow the two subsystems to operate as individual units. This permits separate development of the feed system to proceed simultaneously with optimization of the newly constructed thruster before the thruster system is integrated. Integration is scheduled sufficiently early in the program so that the integrated thruster system can be tested and its performance can be optimized prior to completion of this contract.

SECTION VI

RECOMMENDATIONS AND FUTURE PLANS

During the next quarter the program will continue along the following lines:

- The 20 cm thruster employing an externally cooled LM cathode will continue to be modified in an effort to improve thruster performance in the beam current range from 0.5 A to 1.0 A. The discharge-chamber configuration which is found to yield optimum performance in this thruster will be employed as the initial configuration of the 20 cm thermally integrated LM cathode thruster.

- The 20 cm LM cathode thruster system will be assembled and tested. As necessary, elements of the thruster system will be modified in order to optimize its operation with respect to thruster stability and operating efficiency, ease and reliability of feed-system operation, and thermal compatibility of all components.

- Thermal analysis, using computer program TAS-1B, will continue with emphasis on optimizing the thermal design of the 20 cm thruster system.

- Flow-bench calibration of the liquid-mercury flowmeter will be discontinued; its testing will continue as part of the LM cathode thruster system. A Whittaker Model PACE P 109 D pressure transducer (weighing 0.098 kg) will be substituted for the much heavier Winsco Model PB415 transducer used earlier. The flowmeter impedance SC-5 will be baked in vacuum before mercury is re-introduced.

- The EM pump will be tested further to establish the long-term wetting characteristics of the three metals proposed for the electrode material.

- Improved procedures will be instituted to assure complete outgassing of both the feed system components and the mercury liquid. These precautions are expected to contribute significantly toward stabilizing the operating characteristics of both the EM pump and the liquid-mercury flowmeter.

- Construction and testing of the high-voltage isolator will continue along the lines described in this report.

SECTION VII

NEW TECHNOLOGY

During the first quarter of the current phase of this contract, an invention which is believed to be patentable was reduced to practice. Accordingly, the following patent disclosure was submitted to the Patent Department of the Hughes Aircraft Company.

PD 69419, Sensitive Liquid-Metal Flow Meter, by Julius Hyman, Jr.

The principles upon which this invention is based are reported to NASA on pp. 21-23 of the First Quarterly Report, 15 May 1968, covering Phase I of this contract. Further details concerning the theory of operation of this device are contained in the Appendix of the present report.

REFERENCES

1. J. Hyman, Jr., W. O. Eckhardt, J. R. Bayless, J. A. Snyder, and J. W. Pfeifer, "High-Temperature LM Cathode Ion Thrusters," Final Report, Contract JPL 952131, Hughes Research Laboratories, 1969.

2. Liquid Metals Handbook, U.S. Government Printing Office, 2nd Ed., 165, (June 1954).
   J. Nejedlik and E. Vargo, "Material Resistance to Mercury Corrosion," Electrochemical Technology, Vol. 3, pp. 9-10, 250 (1965).
   W. Latimer and J. Hildebrand, Principles of Chemistry and Reference Book of Inorganic Chemistry (Macmillan, New York, 1940), p. 490.
   H. Logan, The Stress Corrosion of Metals (Wiley, New York, 1966), p. 193.
   H. Uhlig, The Corrosion Handbook (Wiley, New York, 1948), p. 618.
   B. Power and F. Robson, "Experiences with Demountable U.H.V. Systems," Tech. Rep. of Edwards High Vacuum Ltd., Crawley, Sussex, England.

3. J. Hyman, Jr., W. O. Eckhardt, J. W. Pfeifer, and J. A. Snyder, "High-Temperature LM Cathode Ion Thrusters," Quarterly Report No. 1, Contract JPL 952131, Hughes Research Laboratories, May 1968; NASA Accession No. N68-27741.

4. J. Hyman, Jr., W. O. Eckhardt, and J. A. Snyder, "High-Temperature LM Cathode Ion Thrusters," Quarterly Report No. 2, Contract JPL 952131, Hughes Research Laboratories, August 1968; NASA Accession No. N68-36658.

5. J. Hyman, Jr., J. R. Bayless, J. A. Snyder, and W. O. Eckhardt, "High-Temperature LM Cathode Ion Thrusters," Quarterly Report No. 3, Contract JPL 952131, Hughes Research Laboratories, November 1968.

6. T. D. Masek and E. V. Pawlik, "Thrust System Technology for Solar Electric Propulsion," AIAA Paper No. 68-541, AIAA 4th Propulsion Joint Specialists Conference, Cleveland, Ohio, June 1968.

7. R. T. Bechtel, "Discharge Chamber Optimization of the Sert II Thruster," AIAA Paper No. 67-668, AIAA Electric Propulsion and Plasmadynamics Conference, Colorado Springs, Colorado, September 11-13, 1967.

8. W. Knauer, "Power Efficiency Limits of Kaufman Thruster Discharges," to be presented at AIAA 8th Aerospace Sciences Meeting, January 1970.

9. W. Knauer, R. L. Poeschel, H. J. King, and J. W. Ward, "Discharge Chamber Studies for Mercury Bombardment Ion Thrusters," Contract NAS 3-9703, Hughes Research Laboratories, September 1968.

10. W. O. Eckhardt, K. W. Arnold, G. Hagen, J. Hyman, Jr., J. A. Snyder, and R. C. Knechtli, "High-Temperature Liquid Mercury Cathodes for Ion Thrusters," Summary Report, Contract No. NASW-1404, Hughes Research Laboratories, July 1967.

11. "Ion Engine Thrust Vector Study," Final Report, Contract JPL 952129, Hughes Research Laboratories, 1968.

12. W. L. Wolfe, Handbook of Military Infrared Technology (Office of Naval Research, Washington, D.C., 1965).

13. J. H. Molitor, H. J. King, and S. Kami, "A Study of Liquid Mercury Isolator Development," Hughes Research Laboratories, Final Report, Contract No. NAS 7-539, September 1967.

APPENDIX

STABILIZATION OF THE FLOWMETER CALIBRATION

The time-varying behavior of the output characteristic of the liquid-mercury flowmeter (described in Section IV) results from a discontinuous flow characteristic which arises from forces caused by surface tension. In Fig. A-1, three sets of diagrams are shown which portray the character of mercury flow as it emerges from a nonwetting constriction such as that which occurs downstream of single-capillary flow impedance SC-5, which is part of the liquid-mercury flowmeter. This situation, shown in Fig. A-1(a), occurs when the mercury emerges from the constriction into a low-pressure region, as is the case with a single-capillary flow impedance which empties into vacuum. A vacuum void can form at the constriction if the hydrostatic pressure at that point is less than the pressure due to surface tension ($p < p_{ST}$). This tendency is related to the reluctance of a nonwetting liquid (mercury on stainless steel) to enter a capillary tube. This reluctance, which arises from surface tension forces, must be overcome by a drive pressure equal to the pressure resulting from surface tension, p_{ST}, which is related inversely to the tube diameter D by the formula*

$$p_{ST} = \frac{4\gamma \cos \theta}{D}$$

where γ is the coefficient of surface tension and θ is the contact angle between the liquid and the tube wall. From Sears* we have (for mercury on most metals)

$$\theta \cong 130°$$

$$\gamma = 473 \text{ dyn-cm}^{-1}.$$

*F. W. Sears, Principles of Physics, I (Addison-Wesley), Reading, Mass., 1947).

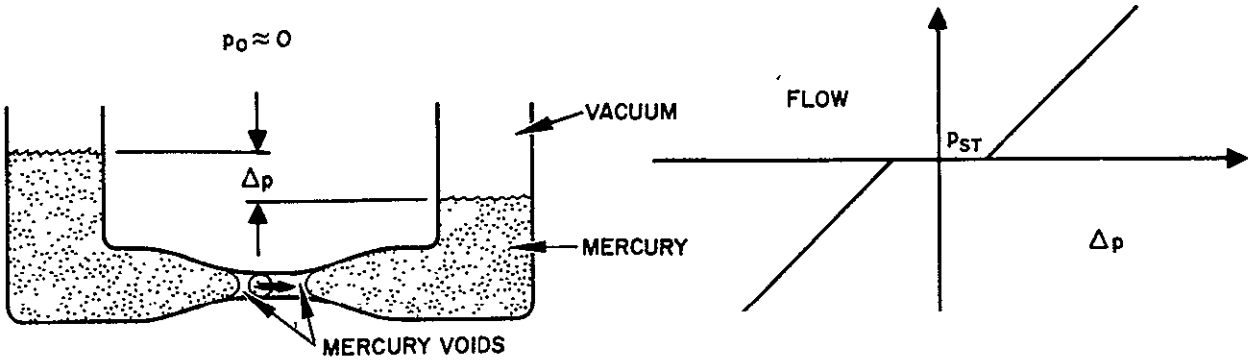

(a) DISCONTINUOUS MERCURY FLOW CHARACTERISTIC WHEN $p_o \approx 0$

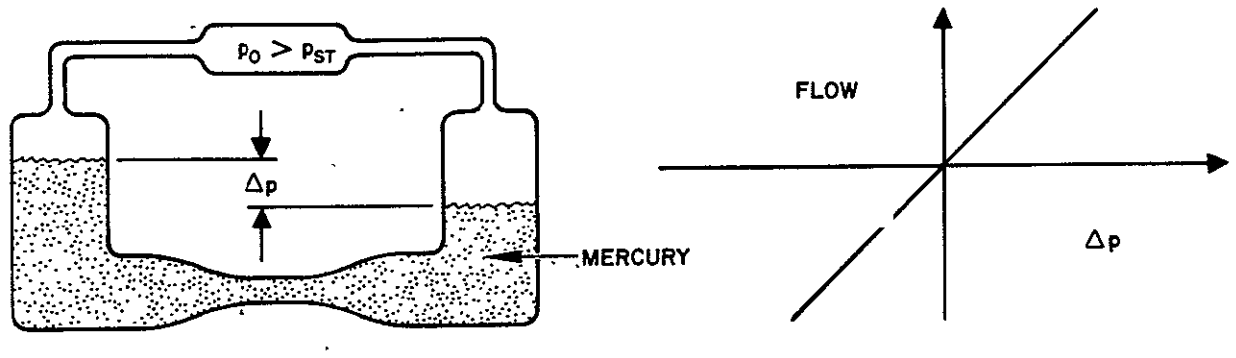

(b) CONTINUOUS MERCURY-FLOW CHARACTERISTIC WHEN $p_o > p_{ST}$

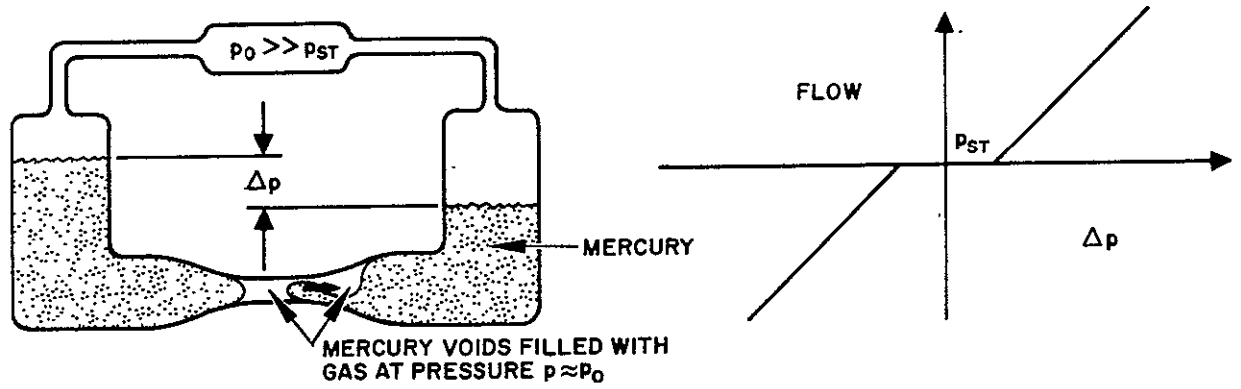

DISCONTINUOUS MERCURY FLOW CHARACTERISTIC WHEN $p_o >> p_{ST}$
BUT GAS BUBBLES ARE PRESENT

Figure A-1.

In convenient units, the formula for this pressure can be re-expressed as

$$p_{ST}\ (\text{psi}) = \frac{1.75 \times 10^{-2}}{D\ (\text{cm})}$$

As illustrated in Fig. A-1(a), this condition results in a discontinuous flow characteristic similar to that which was observed earlier with single-capillary impedance SC-3.*

As shown in Fig. A-1(b), the flow characteristic takes a continuous form if the liquid-mercury flow emerges from the constriction into a region where the hydrostatic pressure is greater than that resulting from surface tension ($p > p_{ST}$); this prevents formation of the vacuum void which was responsible for the discontinuous characteristic. If the flowmeter is located upstream of the simulated cathode impedance SC-3, the flowmeter capillary SC-5, is not subject to the formation of vacuum voids because the hydrostatic pressure is always greater than that due to surface tension over the required range of mercury flowrate from I_a = 0.5 A to 1.0 A.

For zero flowrate, the linear output signal of the transducer (shown in Fig. 14) approaches a value corresponding to a pressure drop of from 1.7 to 2.5 psi (which is similar in magnitude to the pressure due to surface tension which is expected for a capillary having the same diameter SC-5). The presence of the nonzero intercept indicates a return to the discontinuous flow characteristic in spite of the relatively high value of the hydrostatic pressure which prevails within the flowmeter impedance. Return to the discontinuous characteristic at higher pressures is interpreted as indicating the presence of a small gas bubble located at the flow constriction which permits the formation of a gas-filled void. This fosters the same type of discontinuous behavior described earlier. As mercury flows through the constriction, the liquid column breaks repeatedly into segments as the gas bubble breaks through the liquid, to return to its position of stable equilibrium near the center of the constriction. This condition is illustrated in Fig. A-1(c).

---

*J. Hyman, Jr., W. O. Eckhardt, J. R. Bayless, J. A. Snyder, and J. W. Pfeifer, "High-Temperature LM Cathode Ion Thrusters," Final Report, Contract JPL 952131, Hughes Research Laboratories, 1969, Fig. 31.

It is not the mere existence of a nonzero intercept in the flowmeter characteristics, but rather the time variation in the value of the intercept which diminishes the accuracy of this instrument. Over long periods of time the exact value of the pressure p_{ST} can be expected to fluctuate in response to changes in the degree of wetting of the tube-wall surface by the mercury. Such fluctuations have resulted in a shift of flowmeter calibration, which was observed after the first ten data points were acquired. To completely stabilize the calibration characteristic of this flowmeter with respect to fluctuations in the value of p_{ST}, the effects due to surface tension should be eliminated completely by careful elimination of all gas bubbles within the liquid-mercury feed system.